Response to Anonymous Referee #2

We are grateful to the Anonymous Referee #2 for the detailed comments and suggestions which greatly improved the quality of our manuscript. Our manuscript has been revised according to the comments from the Referee and our responses to the comments are as follows. Reviewer comments have been copied (R:) and replied to (A:) below. For clarity, the comments are reproduced in blue, authors' responses are in black and changes in the manuscript are in red.

General comments:

This manuscript describes a system of environmental chamber experiments to examine the kinetics and product distribution both in the gas and aerosol phase from a mixture of DMS and α-pinene. The work describes the non-linear effect of DMS on the oxidation of α-pinene with respect to the mass concentration and yield of SOA. The authors attribute this observation primarily to acid catalyzed heterogeneous reactions and changing OH reactivity and concentrations. The authors present a detailed analysis of the SOA and the components that could be contributing to the observed SOA. The authors also present multiple mechanisms to help explain the observed masses. The work in its current form is confusing and contains errors and issues with the figures and supporting claims. I cannot recommend this publication in its current form. I would request major revisions before publication is reevaluated.

Major comments

R2-1:) The tables and figures throughout the work are confusing. Axes are hard to associate with the data and tables seem to have headers that do not match with the presented data.

A2-1:) Thank you for your valuable suggestion.

The following texts, tables and figures were revised in the new manuscript.

Page 4, Lines 101-102:

All experiments were conducted at temperature of 299 ± 1 K and relative humidity (RH) of 30 – 40%.

Page 5, Line 111:

Table 1. Experimental conditions of the chamber experiments.

Exp. No.	[α-pinene]$_0$[a] ppb	[DMS]$_0$[a] ppb	Δ[α-pinene][b] ppb	Δ[DMS][b] ppb	[NO]$_0$[a] ppb	[NO$_x$]$_0$[a] ppb	[SO$_2$]$_{max}$[c] ppb	[O$_3$]$_{max}$[c] ppb
individual α-pinene								
A-1*	308	0	308	-	195	206	-	21
A-2*	285	0	285	-	201	204	-	30
individual DMS								
D-1	0	184	-	183	189	192	68	19
D-2*	0	290	-	276	206	211	103	25
D-3*	0	600	-	372	207	212	183	41

mix *α*-pinene and DMS								
AD-1	312	140	312	83	208	211	35	25
AD-2	321	197	321	87	190	195	42	25
AD-3	305	301	305	181	203	212	76	23
AD-4	291	372	291	307	183	203	89	18
AD-5	308	441	308	338	193	202	111	25
AD-6	317	536	317	359	191	203	110	24
AD-7	282	639	282	384	196	206	140	27
AD-8	306	613	306	440	189	193	156	45
AD-9	295	687	295	457	183	191	154	51
AD-10*	319	251	319	219	197	200	82	25
AD-11*	314	401	314	330	184	194	116	22
AD-12*	332	646	332	447	198	199	179	26
AD-13*	300	614	300	406	193	197	147	29

[a] Initial concentration of *α*-pinene, DMS, NO and NO_x.
[b] The consumption of *α*-pinene and DMS when the particles were produced to the maximum mass concentration determined by SMPS.
[c] The maximum concentration of O_3 and SO_2 production during light exposure.
* For off-line analysis of SOA. MS Analysis: Exp. A-1, D-2, AD-10, AD-11, AD-12. IR Analysis: Exp. A-2, D-3, AD-13.

Page 9, Line 198:

Table 2. Experimental results of particle-phase components in photooxidation of DMS/*α*-pinene/NO_x systems.

Exp. No.	**[Total particles] [a] μg m^{-3}**	**[H_2SO_4][b] μg m^{-3}**	**[MSA][b] μg m^{-3}**	**[SOA_m][c] μg m^{-3}**	**Y_m[d]**	**[SOA_p][e] μg m^{-3}**
individual *α*-pinene						
A-1	269.5	-	-	269.5	0.16±0.02	
individual DMS						
D-1	177.2	50.8	32.83	116.2	0.25±0.03	
mix *α*-pinene and DMS						
AD-1	296.3	15.0	22.2	270.8	0.14±0.02	216.7
AD-2	422.3	15.7	22.5	400.1	0.20±0.02	270.3
AD-3	572.6	45.4	24.9	507.5	0.24±0.02	425.8
AD-4	714.4	55.4	50.5	607.7	0.25±0.03	648.7
AD-5	683.0	48.8	36.2	613.1	0.24±0.02	708.2
AD-6	551.5	35.3	8.5	504.2	0.19±0.02	680.9
AD-7	539.9	48.4	16.8	476.0	0.19±0.02	677.5
AD-8	364.4	68.7	0.1	237.1	0.08±0.01	537.6
AD-9	289.9	83.2	7.0	154.0	0.06±0.01	436.5

[a] The mass concentration of particles generated by SMPS, corrected for particle wall loss, was calculated as a particle density of 1.2 g cm^{-3}.
[b] IC detection, particle-phase products generated by DMS photooxidation. NH_4^+ was hardly detected. All SO_4^{2-} were detected by IC as H_2SO_4.
[c] The measured SOA mass concentration is expressed as $[\text{Total particles}]_{\text{after-correction}} \times (1 - [H_2SO_4] / [\text{Total particles}]_{\text{before-correction}})$.
[d] $[SOA_m] / (\Delta[\alpha\text{-pinene}] + \Delta[\text{DMS}])$, as mixed yield. Error bars indicate SMPS instrument error of 10%.

Page 7, Line 173:

Table 2 show the experimental results of particle-phase components in photooxidation of DMS and *α*-pinene systems.

Page 8, Lines 185-187:

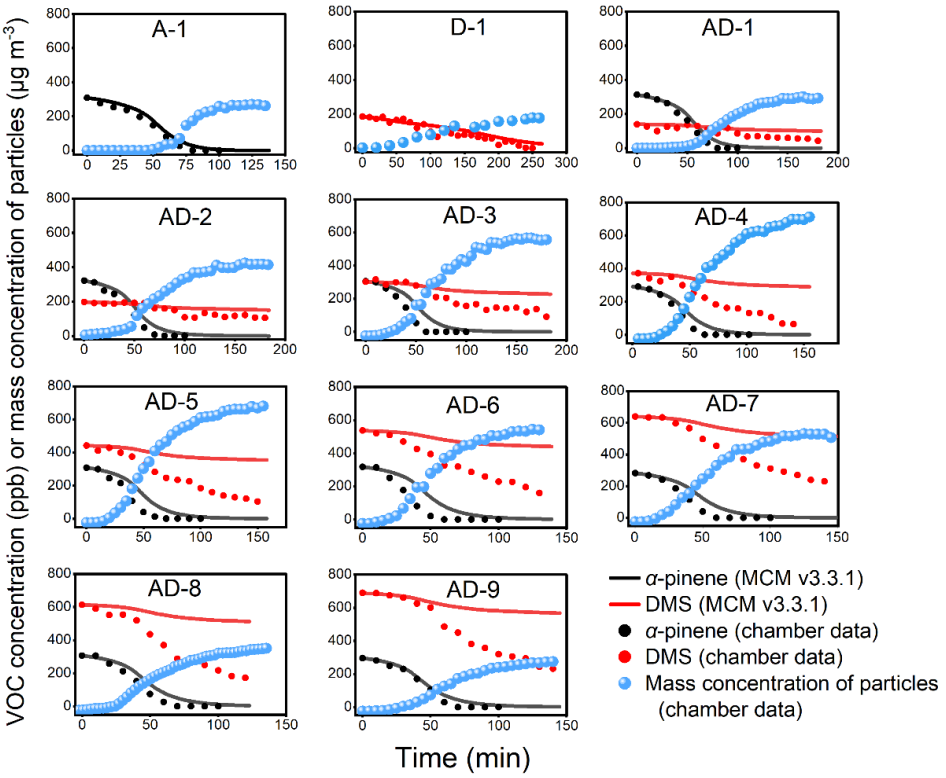

Figure 2. Variation of precursors with reaction time. Red and black dots indicate the results of smog chamber experiments and the curves indicate the results of MCM simulations. Blue dots indicate mass concentration of particles in smog chamber.

Page 14, Lines 299-303:

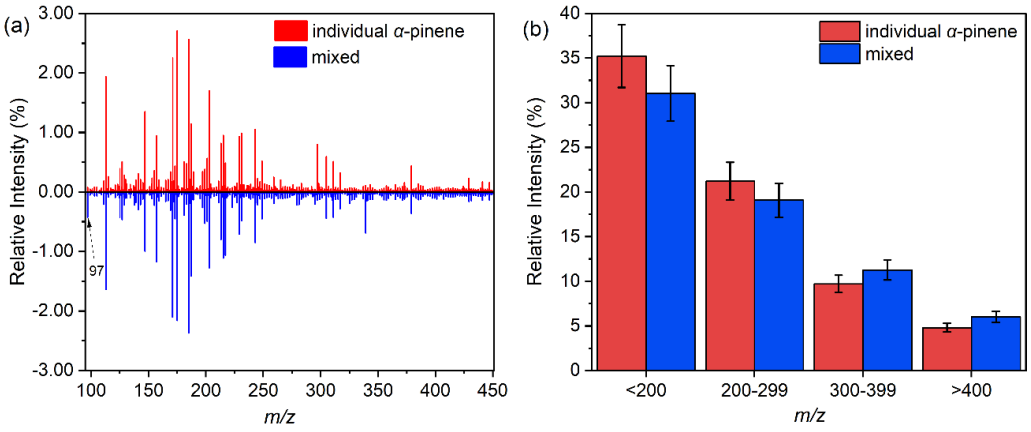

Figure 6. Comparison of negative mode mass peak of SOA in the individual *α*-pinene and mixed systems. (a) Mass spectra of SOA with/without the presence of DMS. (b) Comparison of the relative intensities of mass spectrometry peaks with different *m/z*

ratio ranges. Relative strength is the strength of a substance with a certain mass-to-charge ratio divided by the total strength of all substances.

Page 15, Lines 329-331:

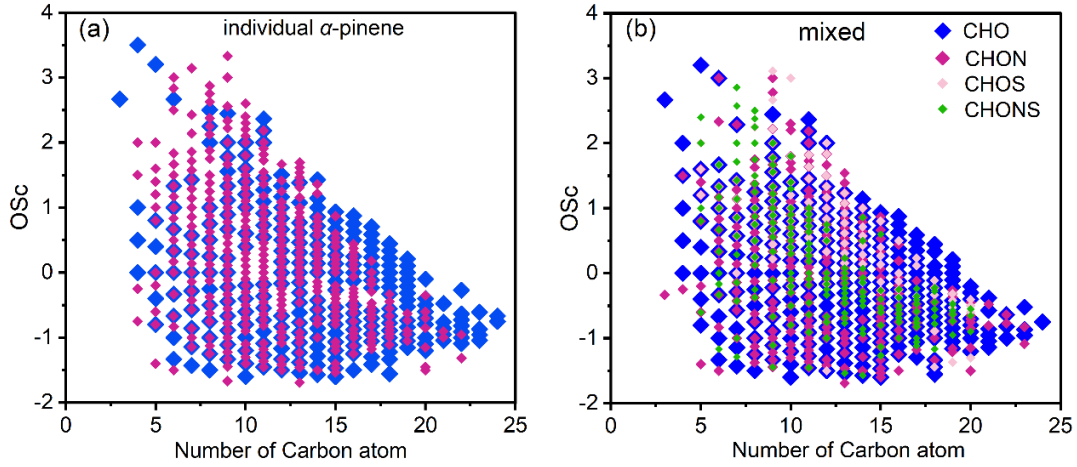

Figure 8. The plots of OS_C against carbon number of particulate organic molecules formed from individual α-pinene (a) and mixed conditions (b).

Page 16, Lines 341-343:

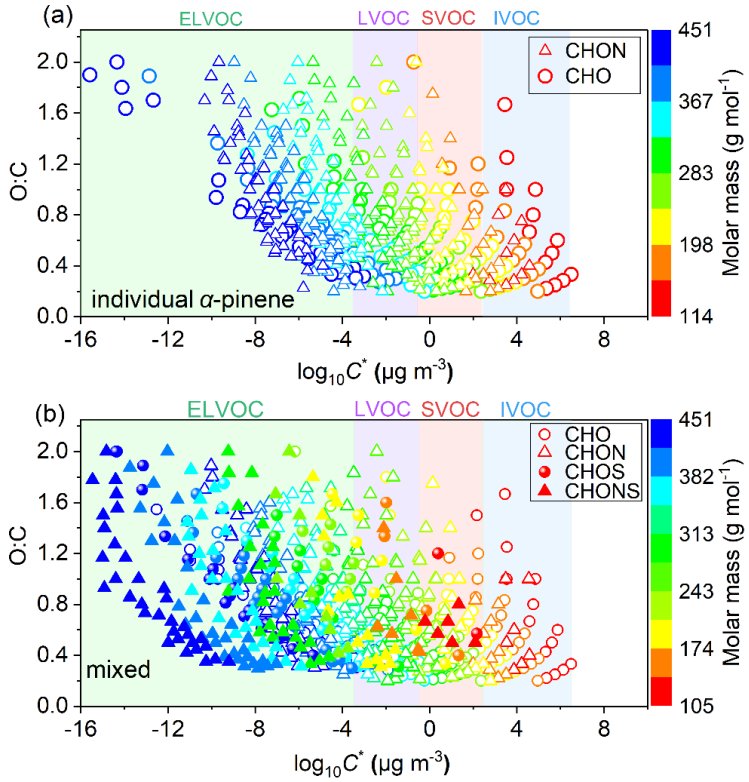

Figure 9. Relationship between O:C and saturation concentration for molecules of different element types in individual α-pinene oxidation (a) and mixed oxidation (b).

Page 17, Lines 360-365:

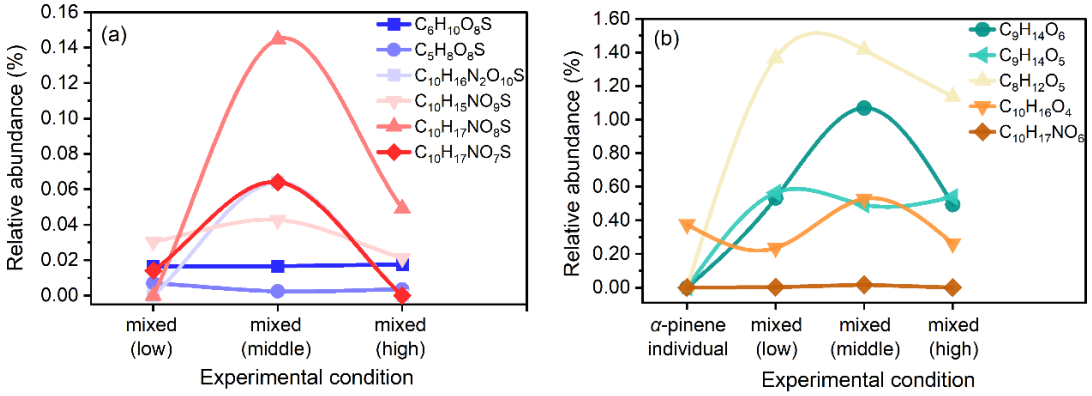

Figure 10. Relative abundance of molecules identified in different reaction systems. (a) S-containing components in the mixed oxidation at different DMS concentrations. (b) CHO/CHON components recognized in individual and mixed oxidation. Details of the molecules are given in Table S4. "Low, medium and high" represent Δ[DMS]/Δ[*α*-pinene] in mixed experiments, indicating different mixing ratios. Specifically, "low" represents Exp. AD-10 below the turning point, "medium" represents Exp. AD-11 at the turning point, and "high" represents Exp. AD-12 below the turning point.

The following figures were added or revised in the new supplement.
SI Page 13, Lines 250-253:

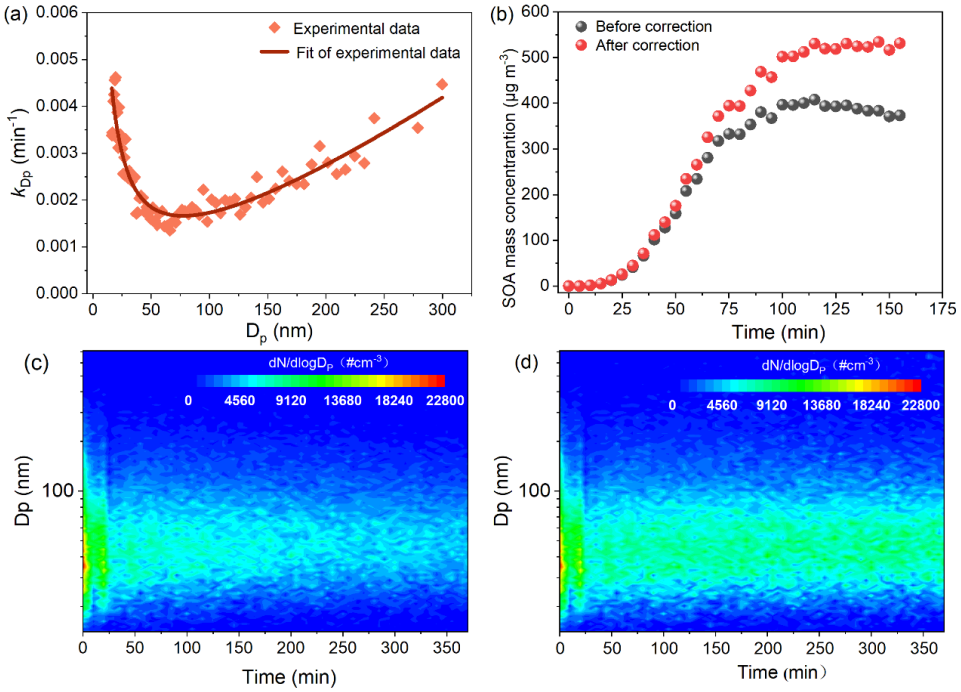

Figure S2. Wall-loss correction of particle. (a) Variation of particle wall-loss coefficient with particle size. (b) Total particle mass concentration of aerosols generated from mixed system. (c) Size-dependent particle number concentration before correction from mixed system. (d) Size-dependent particle number concentration after correction from mixed system.

SI Page 17, Lines 268-269:

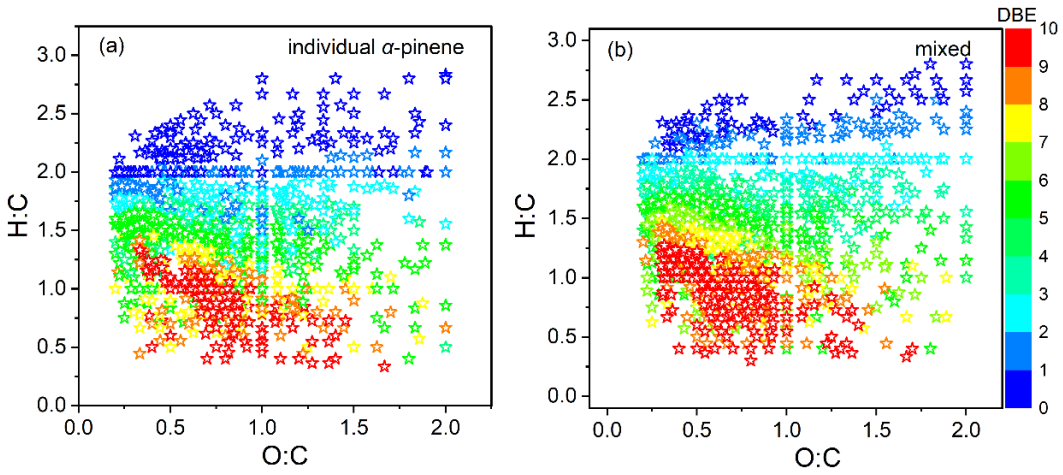

Figure S8. Van Krevelen plots of compounds formed from individual α-pinene (a) and mixed system (b).

R2-2:) The work does a good job trying to disentangle the effect of DMS and alpha-pinene on SOA formation by looking at the products and yields separately as well as in a mixture. The concentrations of VOCs, NO_x and H_2O_2 are atypical of the environment and should be discussed in more detail. I understand limitations of instrumentation and observations, but additional work (facilitated by modeling) could be used to better understand the fate of the VOC and the RO_2 generated from OH oxidation within the chamber.

A2-2:) Thank you for your valuable suggestion. We agree that the fate of the RO_2 generated from OH oxidation is important to be understood in the chamber. Therefore, we evaluate the fate of RO_2 by estimating the relative contribution (percentage) of RO_2 + HO_2, RO_2 + NO and RO_2 + RO_2 reactions. In the quantitative calculations for these three channels, we used the recommended general rate constants (Ziemann and Atkinson, 2012). Although the type of RO_2 and the product channels can bias the results slightly, it is negligible for overall quantification (Peng et al., 2019). We focus on RO_2 in general and do not specifically discuss the chemical characterization of specific RO_2 oxidation products. It is important to note in particular that the RO_2 self- and cross-reaction rate constant is highly correlated with RO_2 type (Peng et al., 2019). Rate constants are highly dependent on the specific RO_2 types and can vary over a very large range (10^{-17} - 10^{-10} cm^3 $molecule^{-1}s^{-1}$). Unsubstituted primary, secondary and tertiary RO_2 radicals self- and cross-reaction rate at ~ 10^{-13}, ~ 10^{-15} and ~ 10^{-17} cm^3 $molecule^{-1}s^{-1}$, respectively (Ziemann and Atkinson, 2012). Substituted RO_2 types have higher reaction rate constants than unsubstituted RO_2 types, which can reach ~10^{-11} cm^3 $molecule^{-1}s^{-1}$. Based on this, our study used relatively moderate levels of rate constants to quantify RO_2 + RO_2 channels. A value of 2.5 × 10^{-13} cm^3 $molecule^{-1}s^{-1}$ was chosen based on Ziemann and Atkinson (2012)'s study. Meanwhile, for the RO_2 + HO_2 and RO_2 + NO channels, we selected the values 1.5 × 10^{-11} cm^3 $molecule^{-1}s^{-1}$ and 9 × 10^{-12}

cm^3 $molecule^{-1}s^{-1}$ (Ziemann and Atkinson, 2012; Peng et al., 2019). The corresponding contents are added in the revised supplement (SI Pages 8-9, Lines 149-160).

With the known reaction rate constants for each channel, we calculated the contribution of the three reaction channels using the following equations (R1) - (R4):

$$C_{RO_2+HO_2,t} = \frac{k_{RO_2+HO_2}[HO_2]_t}{k_{RO_2+HO_2}[HO_2]_t + k_{RO_2+RO_2}[RO_2]_t + k_{RO_2+NO}[NO]_t} \quad (R1)$$

$$C_{RO_2+RO_2,t} = \frac{k_{RO_2+RO_2}[RO_2]_t}{k_{RO_2+HO_2}[HO_2]_t + k_{RO_2+RO_2}[RO_2]_t + k_{RO_2+NO}[NO]_t} \quad (R2)$$

$$C_{RO_2+NO,t} = \frac{k_{RO_2+NO}[NO]_t}{k_{RO_2+HO_2}[HO_2]_t + k_{RO_2+RO_2}[RO_2]_t + k_{RO_2+NO}[NO]_t} \quad (R3)$$

$$\text{Percentage of each channel} = \frac{\sum_{t=0}[RO_2]_t C_{RO_2+HO_2,t} \text{ or } \sum_{t=0}[RO_2]_t C_{RO_2+RO_2,t} \text{ or } \sum_{t=0}[RO_2]_t C_{RO_2+NO,t}}{\sum_{t=0}[RO_2]_t C_{RO_2+HO_2,t} + \sum_{t=0}[RO_2]_t C_{RO_2+RO_2,t} + \sum_{t=0}[RO_2]_t C_{RO_2+NO,t}} \quad (R4)$$

where $C_{RO2+HO2,t}$, $C_{RO2+RO2,t}$ and $C_{RO2+NO,t}$ (s^{-1}) are the rate percentage of the three channels at the given time point (t), respectively. $[HO_2]_t$, $[RO_2]_t$ and $[NO]_t$ (molecule cm^{-3}) represent the concentration simulated in the MCM model at t, respectively. The percentage of each channel refers to the relative percentage of each reaction channel throughout the whole reaction process. $k_{RO2+RO2}$ = 2.5 × 10^{-13} cm^3 $molecule^{-1}$ s^{-1}, $k_{RO2+HO2}$ = 1.5 × 10^{-11} cm^3 $molecule^{-1}$ s^{-1}, k_{RO2+NO} = 9 × 10^{-12} cm^3 $molecule^{-1}$ s^{-1}. The corresponding contents are added in the revised supplement (SI Page 8, Lines 142-148)

The calculation results are displayed in Fig. R1a below. The reaction pathway with the largest contribution is RO_2 + NO (~50-80%), indicating that our experiments are under the typical high-NO_x conditions. Even though the concentration of VOCs are atypical in the real atmosphere, it can be seen that the percentage of the RO_2 + RO_2 reaction pathway is very low (<10%). This indicates that the RO_2 self- or cross-reaction pathway is a minor fate in our chamber experiments. The corresponding contents are added in the revised supplement (SI Page 9, Lines 161-164; SI Page 18, Lines 273-275).

In addition to the three bimolecular reaction pathways (i.e. RO_2 + RO_2, RO_2 + HO_2 and RO_2 + NO), RO_2 isomerization is also an important reaction pathway. To determine whether isomerization can occur in different reaction systems, we calculated RO_2 bimolecular lifetimes (τ) (Xu et al., 2019), as shown in Equation (R5):

$$\tau = \frac{1}{k_{RO_2+HO_2}[HO_2]_t + k_{RO_2+RO_2}[RO_2]_t + k_{RO_2+NO}[NO]_t} \quad (R5)$$

An RO_2 lifetime (without RO_2 isomerization included) of 10 s leads to a relative importance of isomerization of 50% in the total fate (including all loss pathways) of RO_2 with an isomerization rate constant of 0.1s^{-1}, which is a typical order of magnitude for isomerization rate constants of multifunctional RO_2 with hydroxyl and hydroperoxy substituents (Crounse et al., 2013; D'ambro et al., 2017; Praske et al., 2018). Peng et al. (2019) used models to simulate the atmospheric lifetime of RO_2 in several typical ambient sites, chambers and flow tubes, with data extracted from (Fry et al., 2013; Martin et al., 2016; Martin et al., 2017; Ryerson et al., 2013; Peng et al., 2016; Mao et al., 2009; Stone et al., 2012; Nguyen et al., 2014). NO measured in Los Angeles during the CalNex-LA campaign (Ortega et al., 2016) was 1 ppb, which would to allow RO_2

to isomerize, even in an urban area. The environmental conditions in this region are similar to our experiments, both in a high-NO_x environment. While 10 s is an important threshold, the conditions that apply are remote clean areas where little RO_2 + NO reaction occurs. The atmospheric lifetime of RO_2 in the Los Angeles area starts at 0.3 s, which coincides with our experimental. Therefore, we used 0.3 s as the threshold to evaluate whether isomerization can occur under high NO_x conditions. It can be found that the RO_2 lifetime of all experimental systems are higher than 0.3 s from the Fig. R1b. Thus, it is likely that the isomerization channel of RO_2 can occur in our experiments. The corresponding contents are added in the revised supplement (SI Page 9, Lines 165-180; SI Page 18, Lines 273-275).

Overall, even though the concentration of VOCs and oxidants in our experimental systems are not typical of the environment, the RO_2 fate can still be considered atmospherically relevant.

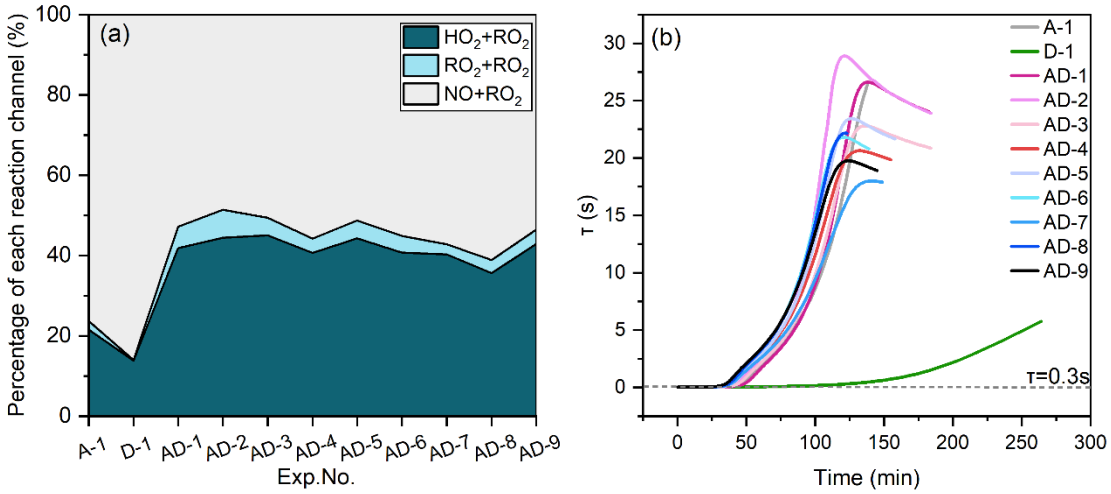

Figure R1. MCM model fitting results for the RO_2 reaction channel. (a) Percentage of different reaction channels of RO_2 in different experiments. (b) Atmospheric lifetime of RO_2 (without RO_2 isomerization included) in different oxidation systems.

Meanwhile, the following texts were added in the revised manuscript.

"In addition, even though the concentrations of VOCs and oxidants in our experimental systems are not typical of the environment, our experiments can still be considered atmospherically relevant. As discussed in detail in Sect. S7, the calculation results indicate that our experiments were conducted under typical high NO_x conditions. Although VOC concentrations are high, RO_2 + RO_2 reaction is not a major fate of RO_2. RO_2 isomerization can likely occur in our experiments as well." (Page 4, Lines 103-107)

R2-3:) Overall the experimental set up and design of the chamber experiments needs to be discussed in more detail, so the reader can understand the observations better. In particular the design of the chamber is not communicated well. There is some general confusion about the [OH] concentration within the chamber and how that plays into the observations of DMS and α-pinene. The DMS observations across the chamber results

seem to have a linear and unmatched decay compared to that of the model. This is a significant fraction of mass that the model is not capturing that is not addressed in the text. A further discussion on limitations or missing mechanisms within the DMS mechanism should be communicated to better understand the present results and subsequent understanding on DMS's effect on SOA yields.

A2-3:) Thank you for your valuable suggestion. We calculated the average OH concentration by the decay of measured DMS concentration in the chamber. We found that the trend of OH concentration in different oxidation systems was consistent with the yield, and all of them showed an increasing and then decreasing trend. The change in OH concentration is likely due to the OH regeneration from the isomerization of $CH_3SCH_2O_2$ radical. The $CH_3SCH_2O_2$ radical generated from DMS oxidation reacts with NO, RO_2, and HO_2, and also undergoes isomerization reactions to form OH (Jacob et al., 2024; Berndt et al., 2023; Ye et al., 2022). We have added reactions related to the isomerization pathway of the $CH_3SCH_2O_2$ radical to the MCM model (Table R1) (Berndt et al., 2020; Ye et al., 2022; Jernigan et al., 2022; Lv et al., 2019; Jacob et al., 2024; Chen et al., 2021; Berndt et al., 2023; Veres et al., 2020; Assaf et al., 2023).

Table R1. Mechanisms related to DMS added to the MCM model.

Reaction	**Rate constant**
$CH_3SCH_2O_2 = HOOCH_2SCH_2O_2$	$2.39\times10^{9}\times e^{-7278/T}$
$HOOCH_2SCH_2O_2 = HPMTF + OH$	$6.10\times10^{11}\times e^{-9.5\times10\text{^}3/T+1.1\times10\text{^}8/T\text{^}3}$
$HOOCH_2SCH_2O_2 + NO = HOOCH_2SCH_2O + NO_2$	$4.90\times10^{-12}\times e^{260/T}$
$HOOCH_2SCH_2O_2 + HO_2 = HOOCH_2SCH_2OOH$	KRO2HO2×0.387
$HOOCH_2SCH_2O_2 + NO_3 = HOOCH_2SCH_2O + NO_2$	KRO2NO3
$HOOCH_2SCH_2O_2 = HOOCH_2SCH_2O$	$3.74\times10^{-12}\times[RO_2]\times0.8$
$HOOCH_2SCH_2O_2 = HOOCH_2SCH_2OH$	$3.74\times10^{-12}\times[RO_2]\times0.91$
$HOOCH_2SCH_2O_2 = HPMTF$	$3.74\times10^{-12}\times[RO_2]\times0.09$
$HOOCH_2SCH_2O = HOOCH_2S + HCHO$	1.00×10^{6}
$HPMTF + OH = HOOCH_2S + CO$	$1.75\times10^{-11}\times0.09$
$HPMTF + OH = OH + HCHO + OCS$	$1.75\times10^{-11}\times0.92$
$HPMTF = HOOCH_2S + HO_2 + CO$	2.10×10^{-11}
$HOOCH_2SCH_2OH + OH = HPMTF + HO_2$	2.78×10^{-11}
$HOOCH_2SCH_2OOH + OH = HOOCH_2SCH_2O_2$	$2.00\times3.68\times10^{-13}\times e^{635/T}$
$OCS + O = CO + SO$	$2.10\times10^{-11}\times e^{-2200/T}$
$OCS + OH = SO + OH$	$7.20\times10^{-14}\times e^{-1070/T}$
$SO = SO_2 + O$	$1.60\times10^{-13}\times e^{-2280/T}\times[O_2]$
$SO + O_3 = SO_2$	$3.40\times10^{-12}\times e^{-1100/T}$
$SO + NO_2 = SO_2 + NO$	1.40×10^{-11}
$SO + OH = SO_2 + HO_2$	$2.60\times10^{-11}\times e^{330/T}$
$HOOCH_2S + O_3 = HOOCH_2SO$	$1.50\times10^{-12}\times e^{360/T}$
$HOOCH_2S + NO_2 = HOOCH_2SO + NO$	$3.00\times10^{-11}\times e^{240/T}$
$HOOCH_2S = HOOCH_2SOO$	$1.20\times10^{-16}\times e^{1580/T}\times[O_2]$
$HOOCH_2SOO = TPA + HO_2$	$7.13\times10^{-31}\times T^{14.02}\times e^{-2556/T}$

Reaction	Rate constant
$HOOCH_2SOO = HOOCH_2S$	1.50×10^{5}
$HOOCH_2SOO = SO_2 + HCHO + OH$	5.00
$TPA + OH = OCS + OH$	$5.00\times10^{-11}\times0.14$
$TPA + OH = OCHSOH + OH$	$5.00\times10^{-11}\times0.86$
$OCHSOH + OH = OCS + OH$	1.40×10^{-12}
$HOOCH_2SO + O_3 = SO_2 + HCHO + OH$	4.00×10^{-13}
$HOOCH_2SO + NO_2 = SO_2 + HCHO + OH + NO$	1.20×10^{-11}
$OCH_2SCH_2OH = HOCH_2S + HCHO$	1.00×10^{6}
$HOCH_2S + O_3 = HOCH_2SO$	$1.50\times10^{-12}\times e^{360/T}$
$HOCH_2S + NO_2 = HOCH_2SO + NO$	$3.00\times10^{-11}\times e^{240/T}$
$HOCH_2S = HOCH_2SOO$	$1.20\times10^{-16}\times e^{1580/T}\times[O_2]$
$HOCH_2SOO = HOCH_2S$	1.50×10^{5}
$HOCH_2SOO = SO_2 + HCHO + HO_2$	5.00
$HOCH_2SO + O_3 = SO_2 + HCHO + HO_2$	4.00×10^{-13}
$HOCH_2SO + NO_2 = SO_2 + HCHO + HO_2 + NO$	1.20×10^{-11}
$OCH_2SCHO = HCHO + OCS + HO_2$	1.00×10^{6}

We evaluate the absolute amount of the isomerization channel of the $CH_3SCH_2O_2$ radical using the MCM model. The corresponding contents are added in the revised manuscript (Page 12, Lines 267-272; Page 13, Lines 273-277, 284-286) and supplement (SI Pages 7-8, Lines 128-141). The parameters related to each reaction channel of the $CH_3SCH_2O_2$ radical generated by DMS oxidation were calculated as shown in equations (R6) - (R11):

$$v_{CH_3SCH_2O_2+X,t} = k_{CH_3SCH_2O_2+X}[X]_t \quad (R6)$$

$$C_{CH_3SCH_2O_2+X,t} = \frac{v_{CH_3SCH_2O_2+X,t}}{v_{Isom.} + \sum_{X=NO/RO_2/HO_2} v_{CH_3SCH_2O_2+X,t}} \quad (R7)$$

$$C_{Isom.t} = \frac{v_{Isom.}}{v_{Isom.} + \sum_{X=NO/RO_2/HO_2} v_{CH_3SCH_2O_2+X,t}} \quad (R8)$$

$$\text{Percentage of } CH_3SCH_2O_2\text{+X' channel} = \frac{\sum_{t=0} C_{CH_3SCH_2O_2+X,t}[CH_3SCH_2O_2]_t}{\sum_{t=0} C_{Isom.t}[CH_3SCH_2O_2]_t + \sum_{X=NO/RO_2/HO_2} (\sum_{t=0} C_{CH_3SCH_2O_2+X,t}[CH_3SCH_2O_2]_t} \quad (R9)$$

$$\text{Percentage of Isom.' channel} = \frac{\sum_{t=0} C_{Isom.t}[CH_3SCH_2O_2]_t}{\sum_{t=0} C_{Isom.t}[CH_3SCH_2O_2]_t + \sum_{X=NO/RO_2/HO_2} (\sum_{t=0} C_{CH_3SCH_2O_2+X,t}[CH_3SCH_2O_2]_t} \quad (R10)$$

$$\text{Amount of Isom.} = \sum_{t=0} C_{CH_3SCH_2O_2+X,t}[CH_3SCH_2O_2]_t \quad (R11)$$

where X denotes the concentration of NO, RO_2, or HO_2 (molecule cm^{-3}) at time t fitted by the MCM model in each experiment. $v_{CH3SCH2O2+X,t}$ denotes the rate (s^{-1}) at which the bimolecular reaction ($CH_3SCH_2O_2$ + NO / RO_2 / HO_2) at time t, respectively. $k_{CH3SCH2O2+X}$ denotes the rate constant (molecule cm^{-3} s^{-1}) for the reaction of the $CH_3SCH_2O_2$ radical with NO, RO_2 or HO_2 at time t, respectively. The rate constants

are respectively (Jacob et al., 2024): $k_{CH3SCH2O2+NO}$ = 1.169 × 10^{-10} molecule cm^{-3} s^{-1}, $k_{CH3SCH2O2+RO2}$ = 3.740 × 10^{-12} molecule cm^{-3} s^{-1}, $k_{CH3SCH2O2+HO2}$ = 5.805 × 10^{-12} molecule cm^{-3} s^{-1}. $\nu_{Isom.}$ is a constant, here assumed to be 0.06 s^{-1} (Jacob et al., 2024; Assaf et al., 2023). $C_{CH3SCH2O2+X,t}$ (%) denotes the rate percentage of the three bimolecular reaction channels at time t. $C_{Isom.t}$ (%) denotes the rate percentage of the isomerization reaction channel. $[CH_3SCH_2O_2]_t$ (molecule cm^{-3}) denotes the concentration of $CH_3SCH_2O_2$ radical at moment t. The percentage of $CH_3SCH_2O_2$ + X'channel or Isom.'channel (%) indicates the relative percentage of a particular bimolecular or isomerization reaction channel throughout the whole reaction process. Amount of Isom. (molecule cm^{-3}) denotes the absolute amount of the isomerization channel throughout the reaction process.

The simulation results are shown in Fig. R2 below. It can be found that the amount of the isomerization channel increases and then decreases as the ratio of precursor consumption increases. The increase in OHR mentioned in the manuscript leads to a decreasing trend of SOA yield after the turning point. This is directly supported by the amount of the isomerization channel of the model-fitted $CH_3SCH_2O_2$ radical. As the Δ[DMS]/Δ[α-pinene] increases further, the absolute amount of isomerization decreases and OH regeneration is less significant.

This estimation result agrees with the measured SOA mass concentration, SOA yield, and OH concentration trends showing in Fig. 4, with the turning point at the Δ[DMS]/Δ[α-pinene] ratio of ~ 0.6 - 1 (i.e., Exp. AD-3 or AD-4). The slight difference (i.e., turning point at AD-3 vs AD-4) is likely due to the incomplete mechanism for DMS in the MCM model. Nevertheless, the results here suggest that the isomerization reaction intensity controls the OH concentration and therefore SOA formation in the mixed experiments.

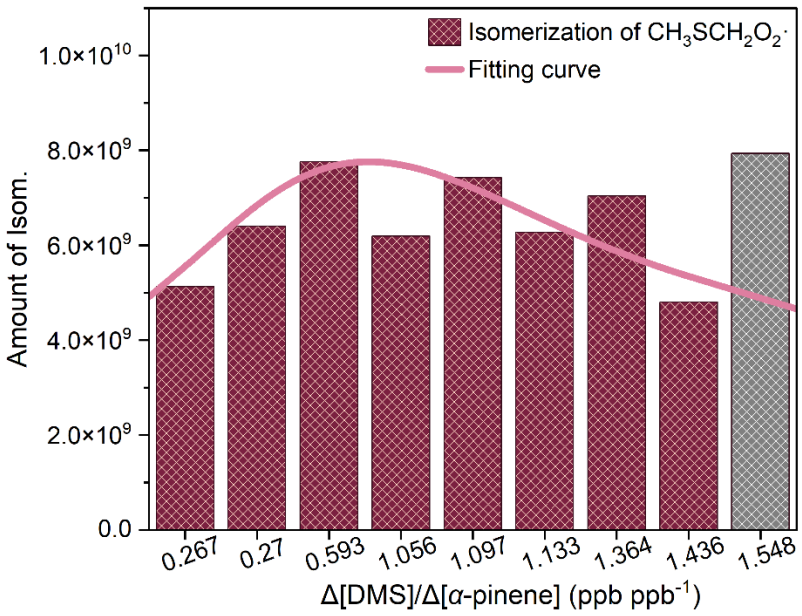

Figure R2. Amount of isomerization channels of $CH_3SCH_2O_2$ radical. A curve was drawn as a guide to the eye. The curve was fitted without using the last data point since it was much higher than the other points.

Elevated OH concentration leads to faster precursors consumption and more SOA generation. We have added details related to the influence of OH concentration on VOCs and SOA in the revised manuscript. As follows:

"OH regeneration before the turning point could attribute to the enhancement in SOA formation. Increasing the average OH concentration within the reaction system helps to enhance the oxidation rates of α-pinene and DMS (Ng et al., 2007), resulting in the rapid generation of low volatile products. The rapid formation of low volatile products ensures the formation and growth of SOA even if there is wall loss of the gas phase products. In addition to this, high OH concentration contributes to multigenerational oxidation reactions (Sarrafzadeh et al., 2016; Robinson et al., 2007; Eddingsaas et al., 2012b). For example, intermediates such as unsaturated keto-aldehydes as well as epoxides can be generated during the photooxidation of α-pinene. Increasing the OH concentration of the reaction system consumes more intermediates, resulting in an increase in the SOA mass concentration. The SOA yield was calculated based on the amount of precursors consumed as well as the SOA mass concentration. Thus the obtained SOA yield is higher at high OH concentration." (Page 12, Lines 250-258)

The large difference between the measured DMS and the modeled DMS is observed in the mixed experiments. This is likely due to the incompleteness of the MCM model for the oxidation mechanism of DMS. We have mentioned the difference in the revised supplement. We elaborate on this reason here as well. The imperfection of the DMS oxidation mechanism in the model and the fact that most studies only focus on the oxidation mechanism of individual species and lack the mechanism of interaction from the overall perspective result in incomplete agreement of the model simulations (Coates and Butler, 2015; Knote et al., 2015; Zong et al., 2018; Yang et al., 2022). In addition, the MCM DMS scheme suffers from a number of problems. Unlike the other VOCs simulated by the MCM (alkanes, alkenes, aromatics, and oxygenates), the DMS scheme has rarely evaluated against chamber experiments. We have incorporated the oxidation mechanism of autoxidation of $CH_3SCH_2O_2$ into the MCM model (Table R1) (Berndt et al., 2020; Ye et al., 2022; Jernigan et al., 2022; Lv et al., 2019; Jacob et al., 2024; Chen et al., 2021; Berndt et al., 2023; Veres et al., 2020; Assaf et al., 2023). However, the MCM DMS scheme is rather outdated (Jacob et al., 2024). In addition, the uncertainty in the gas-phase reaction rate constants of the products of DMS and DMS (Chen and Jang, 2012). The corresponding contents are added in the revised supplement (SI Page 5, Lines 93-102; SI Pages 22-23, Line 300).

Overall, the use of MCM is only supportive. We use this model for the purpose of getting the trend of OH changes in different systems. The vast majority of the results in the manuscript are measured. Although MCM mechanism of DMS is not well established, we believe that the modelled reactivity trend could be used for the comparison with measurements and therefore provide some hints.

We have also added a short description of the gap between the fitted and measured DMS in the revised manuscript. As follows:

"In addition, we also fitted the consumption trends of VOCs with the MCM model. There is some deviation between the measured DMS and the fitted DMS in mixed systems. The reasons for the deviation are detailed in Sect. S5 of the supplement. The time series of inorganic gases and the related presentation of the connection with SOA formation are also presented in Sect. S5 of the supplement." (Pages 8-9, Lines 194–197)

In addition, we have revised the calculation of the average OH concentration in the revised manuscript. As follows:

"The steps for calculating the SOA yield have been mentioned earlier in Table 2." (Page 10, Line 227)

"$[OH]_{avg}$ and OHR were estimated from experimental measurements of VOC concentrations, and their OH reaction rate constants. Detailed calculations are given in Sect. S6." (Page 11, Lines 231-233)

R2-4:) The discussion surrounding OH is confusing and deserves more explanation. In particular, more time needs to be spent describing (or citing) how OH was calculated/constrained within the chamber. Figure 2, presents OH numbers and a trend line, but descriptions of how this was derived is missing. DMS has a well known OH loss rate and is present in most of the experiments, I would recommend using that decay curve to inform your OH concentrations and compare that to your box model results. Additionally, I am confused about the connection between OH loss and aerosol acidity referenced in the work (line 190).

A2-4:) Thank you for your valuable suggestion. **The response regarding OH calculation and the comparison to model can be found above in our response to Comment R2-3.**

We apologize for the confusion caused by the use of the phrase "In addition to acid catalysis". We would like to clarify that DMS affects SOA generation not only through acid catalysis, but also through its own actions such as OH regeneration. In the new manuscript, we have removed this sentence. The trends in OH simulated by the MCM model were described in the original manuscript. We have also presented these texts in the revised manuscript. It is shown below:

"To more accurately reflect the $[OH]_{avg}$ of each experiment, we combined the MCM model to calculate the trends of OH concentration in different experiments with time, as shown in Fig. S6. The maximum OH concentration before the turning point from Exp. AD-1 to Exp. AD-4 are higher than those after the turning point from Exp. AD-5 to Exp. AD-9 at the end of experiments. Interestingly, the largest OH concentration formed in Exp. AD-4 during the time period when the OH concentration was rising at the fastest rate from the local magnification graph, which is consistent with the average OH concentration reflected in Fig. 4d. The OH concentrations of other systems are also largely consistent." (Page 12, Lines 244-250)

R2-5:) Overall, there seems to be a lack of citations or validation for some of the comments made throughout the work. In particular, comprehensive citations

referencing mechanisms, techniques and analysis used and previous chamber work is missing.

A2-5:) Thank you for your valuable suggestion. We add more references to the relevant parts. In addition, the introduction mentioned some work related to chamber for simulated oxidation of mixed VOCs.

Page 2, Lines 36, 37, 38, 42 in the revised manuscript. As follows:

The ambient atmosphere is a complex mixture of different organic gases, which can interact and mix to form SOA through the same emission source or in the atmospheric transport (Voliotis et al., 2022; Malik et al., 2018; Luo et al., 2015; Voliotis et al., 2022a). The oxidation of organic gases with other VOCs produces more SOA with monoterpenes or sesquiterpenes in the mixed systems (Vivanco et al., 2011; Vivanco et al., 2013; Emanuelsson et al., 2013; Voliotis et al., 2022a; Jaoui et al., 2008).

Special molecular structures can enhance the reactivity of mixed systems and accelerate the rate of oxidant consumption, while making the products tend to polymerize and promoting the particle nucleation (Li et al., 2021; Ylisirniö et al., 2020; Yang et al., 2019; Salvador et al., 2020; Vizenor and Asa-Awuku, 2018; Dada et al., 2023; Voliotis et al., 2021).

The cited references are shown below:

Voliotis, A., Du, M., Wang, Y., Shao, Y., Alfarra, M. R., Bannan, T. J., Hu, D., Pereira, K. L., Hamilton, J. F., Hallquist, M., Mentel, T. F., and McFiggans, G.: Chamber investigation of the formation and transformation of secondary organic aerosol in mixtures of biogenic and anthropogenic volatile organic compounds, Atmos. Chem. Phys., 22, 14147-14175, 10.5194/acp-2214147-2022, 2022b.

Malik, T. G., Gajbhiye, T., and Pandey, S. K.: Plant specific emission pattern of biogenic volatile organic compounds (BVOCs) from common plant species of Central India, Environ. Monit. Assess., 190, 631, 10.1007/s10661-018-7015-6, 2018.

Luo, Y., Zhu, L., Fang, J., Zhuang, Z., Guan, C., Xia, C., Xie, X., and Huang, Z.: Size distribution, chemical composition and oxidation reactivity of particulate matter from gasoline direct injection (GDI) engine fueled with ethanol-gasoline fuel, Appl. Therm. Eng., 89, 647-655, 10.1016/j.applthermaleng.2015.06.060, 2015.

Voliotis, A., Du, M., Wang, Y., Shao, Y., Bannan, T. J., Flynn, M., Pandis, S. N., Percival, C. J., Alfarra, M. R., and McFiggans, G.: The influence of the addition of isoprene on the volatility of particles formed from the photo-oxidation of anthropogenic–biogenic mixtures, Atmos. Chem. Phys., 22, 13677-13693, 10.5194/acp-22-13677-2022, 2022a.

Vivanco, M. G., Santiago, M., Martínez-Tarifa, A., Borrás, E., Ródenas, M., García-Diego, C., and Sánchez, M.: SOA formation in a photoreactor from a mixture of organic gases and HONO for different experimental conditions, Atmos. Environ., 45, 708-715, 10.1016/j.atmosenv.2010.09.059, 2011.

Vivanco, M. G., Santiago, M., Sánchez, M., Clavero, M. A., Borrás, E., Ródenas, M., Alacreu, F., Vázquez, M., Clemente, E., Porras, R., Muñoz, A., and Stein, A.:

Experimental data on SOA formation from mixtures of anthropogenic and biogenic organic compounds, Atmosfera, 26, 59-73, 10.1016/S0187-6236(13)71062-2, 2013.
Emanuelsson, E. U., Hallquist, M., Kristensen, K., Glasius, M., Bohn, B., Fuchs, H., Kammer, B., Kiendler-Scharr, A., Nehr, S., Rubach, F., Tillmann, R., Wahner, A., Wu, H. C., and Mentel, T. F.: Formation of anthropogenic secondary organic aerosol (SOA) and its influence on biogenic SOA properties, Atmos. Chem. Phys., 13, 2837-2855, 10.5194/acp-13-2837-2013, 2013.
Jaoui, M., Edney, E. O., Kleindienst, T. E., Lewandowski, M., Offenberg, J. H., Surratt, J. D., and Seinfeld, J. H.: Formation of secondary organic aerosol from irradiated α-pinene/toluene/NO_x mixtures and the effect of isoprene and sulfur dioxide, J. Geophys. Res., 113, 10.1029/2007JD009426, 2008.
Li, J., Li, H., Li, K., Chen, Y., Zhang, H., Zhang, X., Wu, Z., Liu, Y., Wang, X., Wang, W., and Ge, M.: Enhanced secondary organic aerosol formation from the photo-oxidation of mixed anthropogenic volatile organic compounds, Atmos. Chem. Phys., 21, 7773-7789, 10.5194/acp-21-7773-2021, 2021.
Ylisirniö, A., Buchholz, A., Mohr, C., Li, Z., Barreira, L., Lambe, A., Faiola, C., Kari, E., Yli-Juuti, T., Nizkorodov, S. A., Worsnop, D. R., Virtanen, A., and Schobesberger, S.: Composition and volatility of secondary organic aerosol (SOA) formed from oxidation of real tree emissions compared to simplified volatile organic compound (VOC) systems, Atmos. Chem. Phys., 20, 5629-5644, 10.5194/acp-20-5629-2020, 2020.
Yang, J., Ji, D., Hu, Y., Min, X., Zhou, X., and Chen, Q.: Cobalt-catalyzed hydroxymethylarylation of terpenes with formaldehyde and arenes, Chem. Sci., 10, 9560-9564, 10.1039/C9SC03747K, 2019.
Salvador, C. M., Chou, C. C. K., Ho, T. T., Tsai, C. Y., Tsao, T. M., Tsai, M. J., and Su, T. C.: Contribution of terpenes to ozone formation and secondary organic aerosols in a subtropical forest impacted by urban pollution, Atmosphere, 11, 1232, 10.3390/atmos11111232, 2020.
Vizenor, A. E. and Asa-Awuku, A. A.: Gas-phase kinetics modifies the CCN activity of a biogenic SOA, Phys. Chem. Chem. Phys., 20, 6591-6597, 10.1039/C8CP00075A, 2018.
Voliotis, A., Wang, Y., Shao, Y., Du, M., Bannan, T. J., Percival, C. J., Pandis, S. N., Alfarra, M. R., and McFiggans, G.: Exploring the composition and volatility of secondary organic aerosols in mixed anthropogenic and biogenic precursor systems, Atmos. Chem. Phys., 21, 14251-14273, 10.5194/acp-21-14251-2021, 2021.

In addition, the following references were added in the revised manuscript.

"The chemical composition of SOA was determined by ultra performance liquid chromatography (UPLC, UltiMate 3000, Thermo Scientific) coupled with quadrupole time-of-flight mass spectrometry (Q-TOFMS, Bruker Impact HD) (Zhang et al., 2016)." (Page 6, Line 136)

"OH regeneration before the turning point could attribute to the enhancement in SOA formation. Increasing the average OH concentration within the reaction system

helps to enhance the oxidation rates of α-pinene and DMS (Ng et al., 2007), resulting in the rapid generation of low volatile products." (Page 12, Line 252)

"In addition to this, high OH concentration contributes to multigenerational oxidation reactions (Eddingsaas et al., 2012b; Sarrafzadeh et al., 2016; Robinson et al., 2007)." (Page 12, Line 255)

"Based on the previous studies (Librando and Tringali, 2005; Kristensen et al., 2014; Yasmeen et al., 2010; Aschmann et al., 1998; Gao et al., 2006), we show the possible formation pathways of some of these typical CHO molecules in Fig. 11." (Pages 17-18, Lines 374-376)

The cited references are shown below:

Zhang, X., Dalleska, N. F., Huang, D. D., Bates, K. H., Sorooshian, A., Flagan, R. C., and Seinfeld, J. H.: Time-resolved molecular characterization of organic aerosols by PILS + UPLC/ESI-Q-TOFMS, Atmos. Environ., 130, 180-189, 10.1016/j.atmosenv.2015.08.049, 2016.

Ng, N. L., Kroll, J. H., Chan, A. W. H., Chhabra, P. S., Flagan, R. C., and Seinfeld, J. H.: Secondary organic aerosol formation from m-xylene, toluene, and benzene, Atmos. Chem. Phys., 7, 3909-3922, 10.5194/acp-7-3909-2007, 2007.

Eddingsaas, N. C., Loza, C. L., Yee, L. D., Chan, M., Schilling, K. A., Chhabra, P. S., Seinfeld, J. H., and Wennberg, P. O.: α-Pinene photooxidation under controlled chemical conditions - Part 2: SOA yield and composition in low- and high-NO_x environments, Atmos. Chem. Phys., 12, 7413-7427, 10.5194/acp-12-7413-2012, 2012b.

Sarrafzadeh, M., Wildt, J., Pullinen, I., Springer, M., Kleist, E., Tillmann, R., Schmitt, S. H., Wu, C., Mentel, T. F., Zhao, D., Hastie, D. R., and Kiendler-Scharr, A.: Impact of NO_x and OH on secondary organic aerosol formation from β-pinene photooxidation, Atmos. Chem. Phys., 16, 11237-11248, 10.5194/acp-16-11237-2016, 2016.

Robinson, A. L., Donahue, N. M., Shrivastava, M. K., Weitkamp, E. A., Sage, A. M., Grieshop, A. P., Lane, T. E., Pierce, J. R., and Pandis, S. N.: Rethinking organic aerosols: Semivolatile emissions and photochemical aging, Science, 315, 1259-1262, 10.1126/science.1133061, 2007.

Librando, V. and Tringali, G.: Atmospheric fate of OH initiated oxidation of terpenes. Reaction mechanism of α-pinene degradation and secondary organic aerosol formation, J. Environ. Manage., 75, 275-282, 10.1016/j.jenvman.2005.01.001, 2005.

Kristensen, K., Cui, T., Zhang, H., Gold, A., Glasius, M., and Surratt, J. D.: Dimers in α-pinene secondary organic aerosol: effect of hydroxyl radical, ozone, relative humidity and aerosol acidity, Atmos. Chem. Phys., 14, 4201-4218, 10.5194/acp-14-4201-2014, 2014.

Yasmeen, F., Vermeylen, R., Szmigielski, R., Iinuma, Y., Böge, O., Herrmann, H., Maenhaut, W., and Claeys, M.: Terpenylic acid and related compounds: precursors for dimers in secondary organic aerosol from the ozonolysis of α- and β- pinene, Atmos. Chem. Phys., 10, 9383-9392, 10.5194/acp-10-9383-2010, 2010.

Aschmann, S. M., Reisseil, A., Atkinson, R., and Arey, J.: Products of the gas phase reactions of the OH radical with α- and β-pinene in the presence of NO, J. Geophys. Res., 103, 25553-25561, 10.1029/98JD01676, 1998.

Gao, S., Surratt, J. D., Knipping, E. M., Edgerton, E. S., Shahgholi, M., and Seinfeld, J. H.: Characterization of polar organic components in fine aerosols in the southeastern United States: Identity, origin, and evolution, J. Geophys. Res., 111, D14314, 10.1029/2005JD006601, 2006.

Technical comments:

R2-6:) Line 46: Emerging work on DMS oxidation has found the formation of a key intermediate, hydroperoxymethyl thioformate (HPMTF). This intermediate is formed via an isomerization reaction and regenerates OH in the process. I would recommend adding context to this reaction and using it to understand the effect of DMS on the chamber observations.

A2-6:) Thank you for your valuable suggestion. We have added background on HPMTF in the introduction section. The following texts and figure were added in the new manuscript.

"During the daytime, DMS is consumed mainly by the reaction with OH, with H atom-abstraction reaction accounting for 65% (Berndt et al., 2019). A key branch point in DMS + OH is the methylthiomethylperoxy radical (CH_3SCH_2OO) formed from H-atom abstraction followed by O_2 addition. This subsequent reaction of RO_2 plays a dominant role in the product distribution of DMS. The CH_3SCH_2OO radical can undergo bimolecular or unimolecular reactions (Jacob et al., 2024). Recent studies have identified a key intermediate, hydroperoxymethyl thioformate (HPMTF) (Ye et al., 2022; Veres et al., 2020). HPMTF is formed via secondary isomerization of the CH_3SCH_2OO radical and regenerates the OH radical in the process (Berndt et al., 2019; Wu et al., 2015). In addition, DMS forms the major oxidation products, methanesulfonic acid (MSA), sulfuric acid (H_2SO_4), and sulfur dioxide via bimolecular pathways (with NO, HO_2 and RO_2) (Cala et al., 2023). The H-atom abstraction path of DMS is shown in Fig. 1. These products can contribute significantly to oceanic new particle generation, particle growth, and atmospheric chemical processes (Arquero et al., 2017; Fung et al., 2022)." (Page 2, Lines 50-59)

The scheme of the DMS isomerization channel is also presented in the new manuscript (Page 3, Lines 60-62).

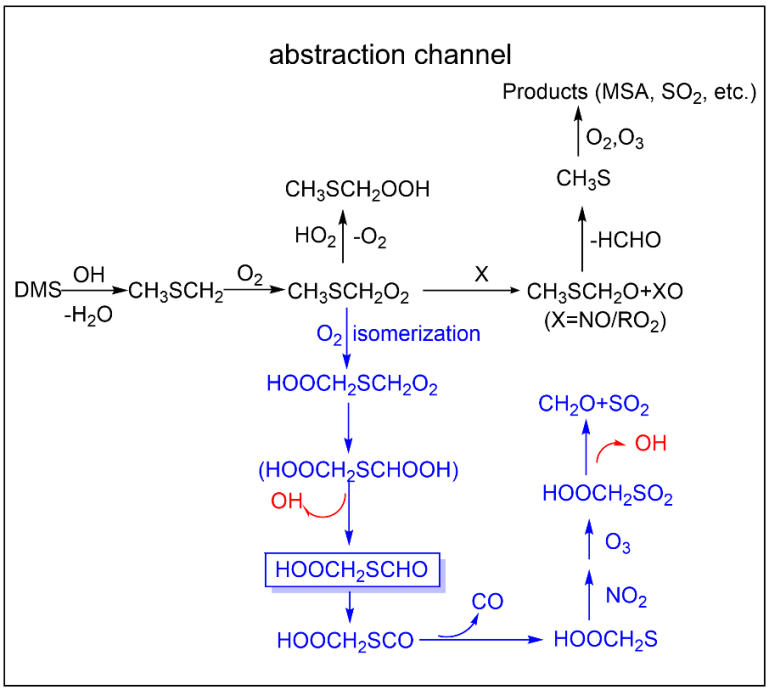

Figure 1. H-abstraction reaction path of DMS with OH, the blue part indicates the intramolecular H-shift of $CH_3SCH_2O_2$ radical, and the red color indicates the formation of OH.

R2-7:) Line 70: How was the chamber run? Is this a batch mode or continuous flow method? Please explain in more detail how the chamber was run and what steps were taken to account for processes like dilution.

A2-7:) All experiments in the chamber were run in the batch mode. Therefore there was no dilution process. In addition, we have added some details of the experiments. The following texts were added in the new manuscript.

"All experiments in the chamber were run in batch mode." (Page 4, Line 85)

"Zero air generated by an air compressor combined with a zero-air generator (Model 1160; Thermo scisentific, USA) was used as the background gas and reactant carrier gas for the simulation experiments." (Page 4, Lines 90-92)

"Following this, hydrogen peroxide (H_2O_2, 30 wt%, Aladdin) was vaporized and flushed into the reactor to serve as a OH radical precursor. The concentration of H_2O_2 in all experiments was controlled at ~300 ppb. NO was introduced into the chamber from a gas cylinder (510 ppm in N_2, Qingdao Deyi Gas Company) using a mass flow controller." (Page 4, Lines 96-99)

"After all the reactants were introduced into the chamber, they were diluted to the desired volume by injecting zero air." (Page 4, Lines 99-100)

"All experiments were conducted at temperature of 299 ± 1 K and relative humidity (RH) of 30 – 40%." (Page 4, Lines 101-102)

R2-8:) Line 83: What are the concentrations of H_2O_2 used in the chamber? You use H_2O_2 photolysis to produce OH under high concentrations of NO. This will lead to a complex and high concentration mixture of HO_2, RO_2 and NO thus changing the fate of the peroxy radical formed in MT and DMS oxidation. Please devote more time to discussing this interaction.

A2-8:) The concentration of H_2O_2 in all experiments was controlled at ~300 ppb. The corresponding contents are added in the revised manuscript (Page 4, Lines 97-98).

Even though we have H_2O_2 as the OH precursor in our reaction systems, the simulation by MCM modeling revealed that the experiment still falls under the typical high NO_x oxidation condition. **The details have been shown in the reply to Comment R2-2.**

R2-9:) Line 100: Wall loss for SOA and VOC can be an important driver of loss within an environmental chamber. Values are given for the wall loss terms without any validation or reasoning for the values. Could the authors please provide context and assumptions made for the values used.

A2-9:) The determination of wall losses of gases and particles is showed in the revised supplement (SI Pages 2-3, Lines 9-37; SI Pages 12-13, Lines 248-253).

(a) Gases

In order to quantify the gas wall loss, the target gas was injected into the clean reactor and its concentration over time was monitored. Wall deposition of gases inside the reactor can be considered as a first-order kinetic process as shown in equation (R12):

$$-\frac{d[C]}{dt} = -k_{ig,w}[C] \quad \text{(R12)}$$

$$\ln\left(\frac{[C]_t}{[C]_0}\right) = -k_{ig,w}t \quad \text{(R13)}$$

where [C] denotes the concentration of gas (ppb). $k_{ig,w}$ denotes the wall loss rate constant of gas (min^{-1}). Further integration of equation (1) leads to equation (R13). $[C]_t$ and $[C]_0$ denote the concentration of inorganic gases at 0 min and t min, respectively. We calculated the first-order wall loss rate constants for α-pinene, DMS, NO, NO_2, SO_2, and O_3 using equation (2). The corresponding values were 3.159×10^{-6}, 8.982×10^{-6},1.178×10^{-6}, 1.241×10^{-6}, 2.878×10^{-6}, and 2.205×10^{-6} min^{-1} (Fig. R3). The calculated values are closer to the inorganic gases in the literature (Wu et al., 2007; Bloss et al., 2005; Metzger et al., 2008). Therefore, the wall losses for the gases are negligible.

(b) Particles

To perform the wall loss correction for the particles, the particles were injected the clean chamber. The number and mass concentrations of SOA produced in the formal experiment were corrected by measuring the wall loss constants of ammonium sulfate particles. Ammonium sulfate particles were generated as follows: ammonium sulfate solid particles were configured as a solution and small ammonium sulfate droplets were generated through an atomizer (Model 3076, TSI), which was then passed through a

silica-gel diffusion dryer and injected into the reactor. After the ammonium sulfate aerosols mixed well with zero air in the reactor, the number and mass concentrations of ammonium sulfate particles were monitored for 6-8 hours using SMPS. We assume that the particle wall loss is a first-order reaction and the particle wall loss rate constant, k_{Dp}, was defined in equation (R14) (Wang et al., 2018). k_{Dp} is related to the particle size and time:

$$\ln[N_{Dp}(t)] = -k_{Dp}t + i \quad \text{(R14)}$$

where N_{Dp} (nm) is the particle number concentration at size D_P and time t, k_{Dp} (h^{-1}) is the first-order particle wall-loss rate constant determined as the slope of the equation, and i is an arbitrary constant. Then, for k_{Dp} at a certain particle size, the four empirical parameters (a, b, c, d) are obtained by fitting with the four-parameter method as shown in equation (R15):

$$k_{Dp} = aD_p^{\,b} + c / D_p^{\,d} \quad \text{(R15)}$$

In this experiment, the parameters a, b, c and d were 1.95×10^{-7}, 1.72, 0.015 and 0.53, respectively. Therefore, the expression for the wall loss rate coefficient can be determined as $k_{Dp} = 1.95 \times 10^{-7} \times D_p^{1.72} + 0.015 \times D_p^{-0.53}$ (Fig. R4a). Then, the corrected SOA number concentration was obtained by equation (R16):

$$V_{Dp}^{\,c}(t) = V_{Dp}^{\,m}(t) + k_{Dp}\int_0^t V_{Dp}^{\,m}(t)dt \quad \text{(R16)}$$

Where $N_{Dp}^{m}(t)$ and $N_{Dp}^{c}(t)$ are measured and corrected particle volume concentration at size D_P. The particle mass concentration was corrected as above. As shown in Fig. R4b and d, the particle mass concentration and number concentration were well corrected.

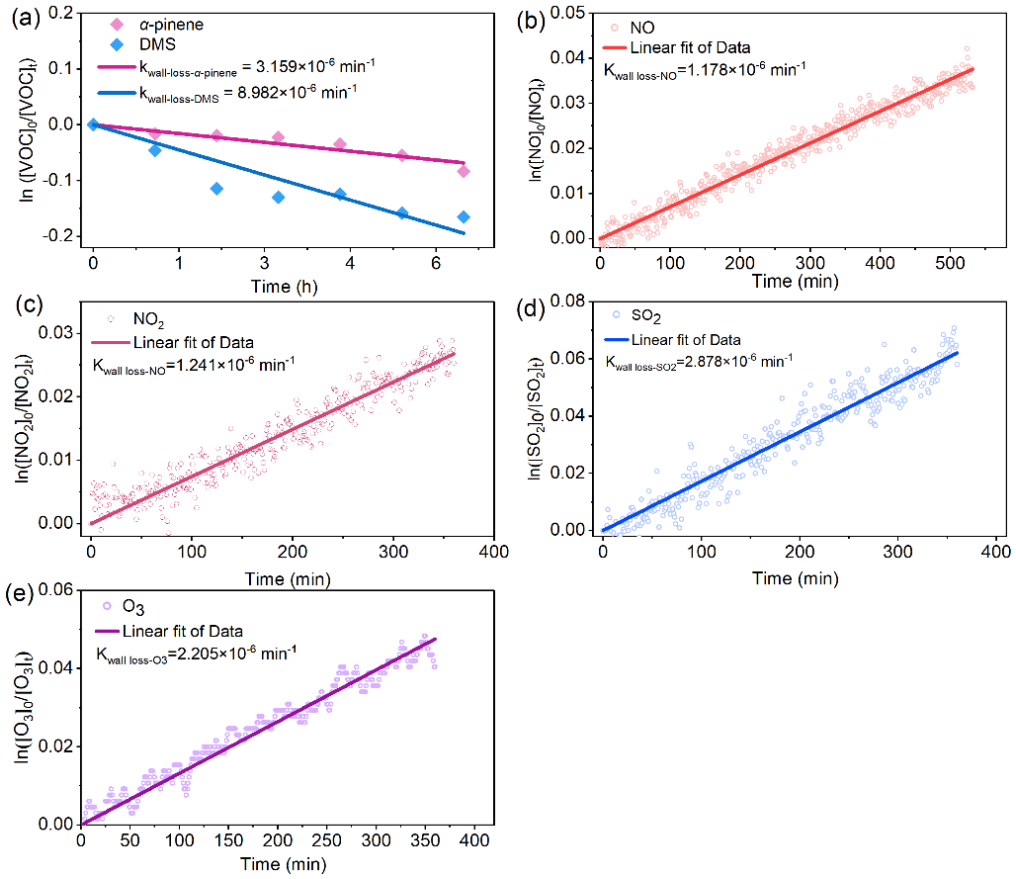

Figure R3. Variation of gas concentration with time. (a) - (e) show the variation of VOC, NO, NO_2, SO_2 and O_3 with time, respectively.

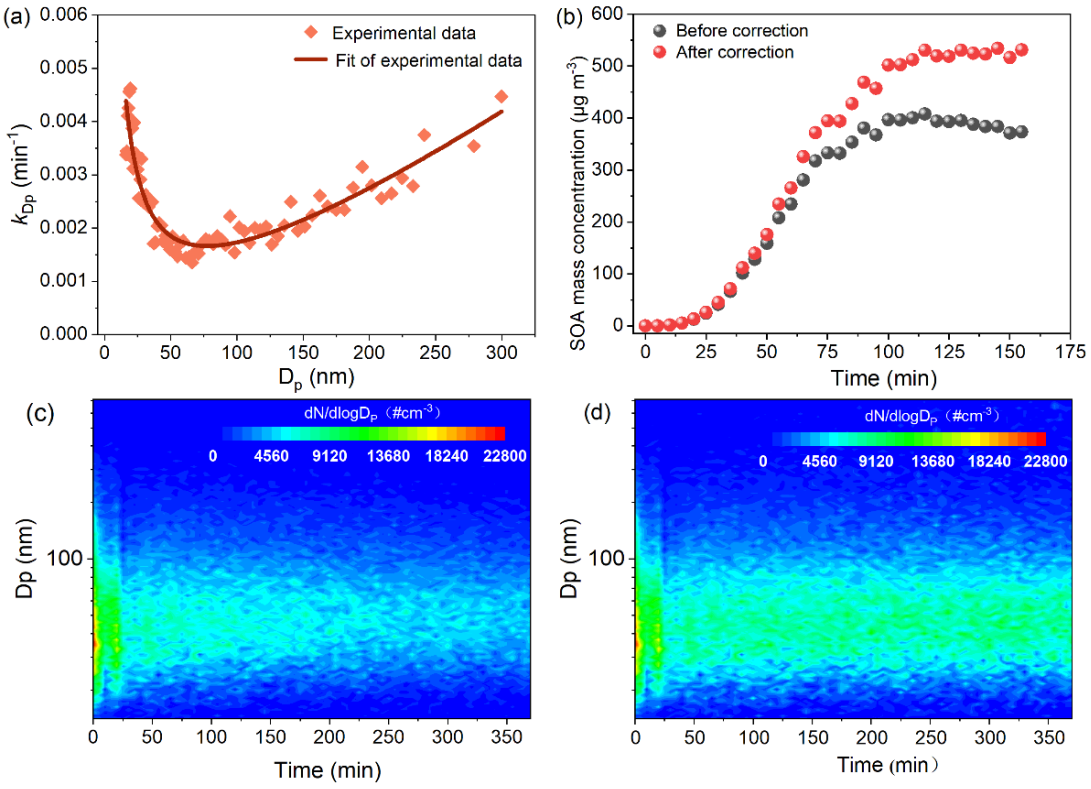

Figure R4. Wall-loss correction of particle. (a) Variation of particle wall-loss coefficient with particle size. (b) Total particle mass concentration of aerosols generated from mixed system. (c) Size-dependent particle number concentration before correction from mixed system. (d) Size-dependent particle number concentration after correction from mixed system.

R2-10:) Figure 1: The axis's colors and labels do not match. I would recommend matching them to guide the readers eye.

A2-10:) Figure 1 (now Figure 2 in the current version) was revised in the manuscript (Page 8, Lines 185-187).

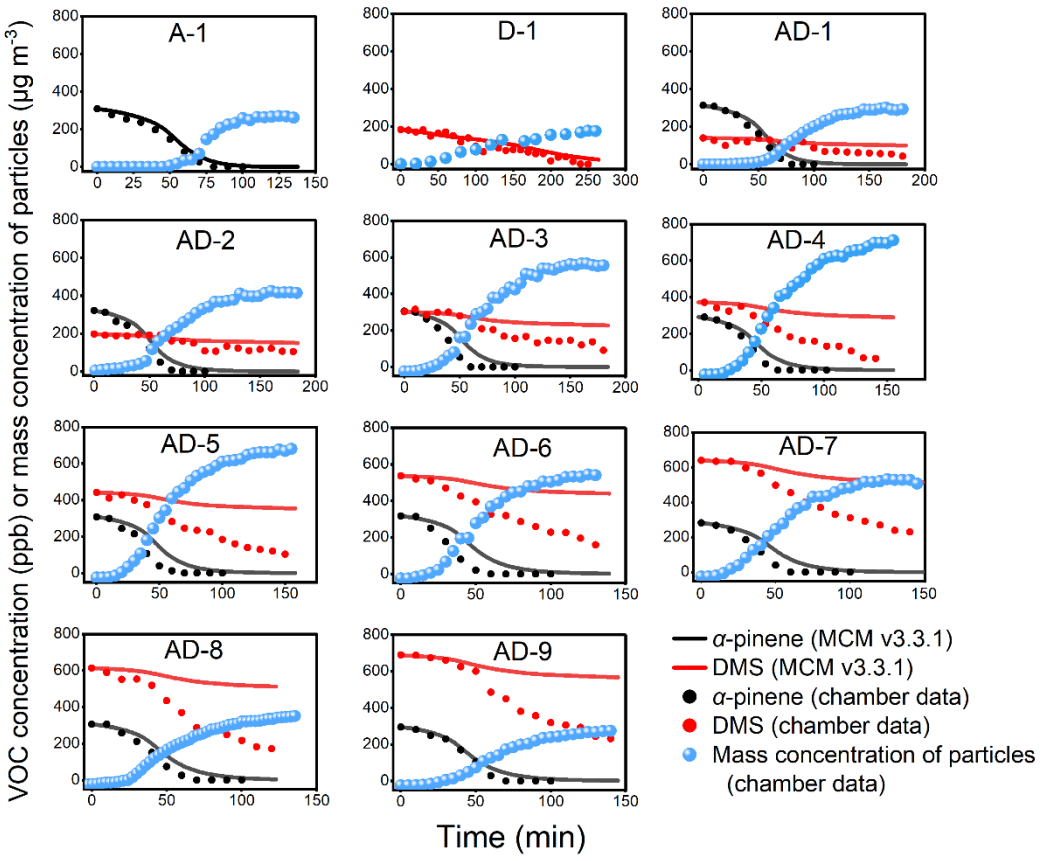

Figure 2. Variation of precursors with reaction time. Red and black dots indicate the results of smog chamber experiments and the curves indicate the results of MCM simulations. Blue dots indicate mass concentration of particles in smog chamber.

R2-11:) Line 150: Can you add a more in-depth analysis of DMS oxidation? You present one DMS chamber experiment and state that your observations don't match with Chen and Jang (2021). DMS has been studied through various oxidation methods and strategies. I would recommend further literature review to see if other work on DMS oxidation can match your observations and if not why. Just stating RH, oxidant and collection method does not explain the observed trends.

A2-11:) Previous studies have shown that the ratio of particulate MSA to non-sea salt sulfate varies between 0.05 and 0.75 and is usually below 0.5 (Bates et al., 1992; Ayers et al., 1996; Chen et al., 2012; Ayers et al., 1991). The ratio of MSA to H_2SO_4 in our study was ~0.67, which was consistent with the actual atmosphere. The multiphase chemical mechanism is complex, and the yields of H_2SO_4 and MSA depend on temperatures well as atmospheric composition (Mauldin Iii et al., 1999; Shen et al.,

2022). Moreover, field measurements of gas-phase MSA and H_2SO_4 show a wide range of concentrations.

In this study, we detected these two typical products of DMS using IC. However, the focus of our study is on the effect of these acidic products of DMS on *α*-pinene SOA via heterogeneous reactions. In addition, DMS itself influences the generation of SOA in the mixed systems through OH regeneration. This aspect of the ratio of MSA to H_2SO_4 is less addressed in our study. To avoid a shift in focus, we have removed the relevant content in the revised manuscript.

If possible, we hope to deeply explore the formation of important products of DMS photooxidation in future studies. We also look forward to further understanding the effect of the ratio of MSA to H_2SO_4 on particulate matter formation.

R2-12:) Line 157: What is SOA in the DMS photooxidation? Could you please elaborate on what the components are of SOA that are not H_2SO_4. Could you please elaborate on what the new particles are in this case? Is the DMS SOA pure sulfuric acid clusters that other DMS derived species build upon. Do you have any indication of NH_3 or a gas-phase base to build with sulfuric acid.

A2-12:) Thank you for your valuable suggestion. DMS-SOA is defined as organosulfur compounds generated by DMS oxidation in the manuscript. Previous environmental monitoring data have shown that particulate matter generated by DMS photooxidation is mainly composed of sulfuric acid and organosulfur compounds. Organosulfur compounds such as DMSO, MSIA, and MSA, as well as other products, are also produced from DMS oxidation via the OH-addition pathway. Many of these products partition into the condensed phase, and extensive data sets exist for methanesulfonate ($CH_3SO_3^-$, MS) and non-sea-salt sulfate (nss-SO_4^{2-}), the deprotonated forms of MSA and H_2SO_4, respectively (Barnes et al., 2006). Methylsulfonylperoxynitrate (MSPN, $CH_3SO_2OONO_2$) have been observed as products of the OH-radical-initiated oxidation of DMS in laboratory studies (Ye et al., 2021).

In fact, we also attempted to utilize UPLC/ESI-Q-TOFMS to detect the particle-phase product of DMS, i.e., Exp. D-2. Unfortunately, we did not detect any valuable signals or substances. We suspect that the insensitivity of the extraction process and program settings of the offline technique to the sulfur-containing products of DMS is the cause. Our exploration of the composition of SOA focuses on the effect of DMS on *α*-pinene SOA, while assuming the particulate phase products of DMS to be typical final products such as H_2SO_4 and MSA. In addition, Chen and Jang (2012) showed that the contribution of detectable H_2SO_4 and MSA, etc., to the offline analysis of the particulate phase products of DMS is not exactly equal to the mass concentration of OM, which is similar to our results. Currently, researchers typically use on-line instruments (e.g., AMS) to detect the particulate phase products of DMS (Ye et al., 2022; Ye et al., 2021). This makes the analysis of the products of DMS more sensitive. We expect that in future studies, the gas-phase and particle-phase components of DMS can be investigated in more detail at the molecular level using AMS, CIMS, etc.

Regarding the form of SO_4^{2-} in the particles, we found that previous studies did not mention the effect of NH_3 on SO_4^{2-}, whether SO_2 or DMS was added as a reactant (Ye et al., 2018; Liu et al., 2019; Lewandowski et al., 2015; Liu et al., 2017). In our experiments, we detected the amount of NH_4^+ in the particulate phase using IC to be between 0.1 and 0.5 μg m^{-3} in the presence of DMS. The concentration of NH_4^+ was 1 to 3 orders of magnitude lower than the mass of the other products of DMS. Alternatively, very small amounts of ammonium sulfate clusters do not affect the mass concentration of SOA. Therefore, we have neglected the effect of NH_4^+ on SO_4^{2-}. We concluded that all SO_4^{2-} quantified by ion chromatography is H_2SO_4 in our experiments.

We attribute particle nucleation to two aspects.

H_2SO_4 affects the formation of particulate matter (Vivanco et al., 2013; Liu et al., 2016). The role of H_2SO_4 in new particle formation has been well studied in previous studies (Berndt et al., 2005; Zhang et al., 2012; Sipilä et al., 2010; Kirkby et al., 2011; Almeida et al., 2013). H_2SO_4 promotes the formation of new particles by participating in nucleation or forming organosulfates. H_2SO_4 increases particle mass concentration and LVOC production via heterogeneous reactions (Xu et al., 2021; Zhang et al., 2023). We detected a certain amount of SO_4^{2-} using IC, which is attributed to H_2SO_4.

LVOCs/ELVOCs formed during reactions were previously found to be involved in the new particle formation (Wildt et al., 2014; Kirkby et al., 2016) and growth of particles, such as highly oxidized multifunctional molecules (HOMs), dimers, and trimers, etc. (Ehn et al., 2014; Kirkby et al., 2016). HOMs of C_8 - C_{10} were identified in our study. These molecules are important for new particle generation.

The corresponding contents are added in the manuscript.

"Previous environmental monitoring data have shown that particulate matter generated by DMS photooxidation is mainly composed of H_2SO_4 and organosulfur compounds (Gaston et al., 2010; Chen and Jang, 2012; Veres et al., 2020). Organosulfur compounds such as DMSO and MSA, as well as other products, are also produced from DMS oxidation via the OH-addition pathway. Many of these products partition into the condensed phase (Barnes et al., 2006). We attempted to utilize UPLC/ESI-Q-TOFMS to detect other particle-phase products of DMS. Unfortunately, we did not detect any valuable signals or substances. We suspect that the insensitivity of the extraction process and program settings of the offline technique to the sulfur-containing products of DMS is the cause." (Page 8, Lines 178-184)

"The particulate matter generated by DMS photooxidation mainly contains two types of components, H_2SO_4 and SOA (or organosulfur compounds)." (Page 8, Lines 188-189)

"[b] IC detection, particle-phase products generated by DMS photooxidation. NH_4^+ was hardly detected. All SO_4^{2-} were detected by IC as H_2SO_4." (Page 9, Line 198)

R2-13:) Table 2: The connection between max O_3, SO_2, and NO_x and max SOA is not a straight forward concept that should be evaluated within the text. Presenting one or two of the time traces could be an informative way to understand when the peaks are occurring and how that relates to the steady state or end of experiment concentration. The amount of O_3 produced across the experiments varies by a decent amount. I would

recommend addressing this variability and seeing if its formation can help understand what is happening within the chamber. Also is O_3 + MT important at these concentrations?

A2-13:) Thank you for your valuable suggestion. We discussed the relationship between inorganic gases and SOA generation in our experiments in Sec. S5 of the original supplement. The trend of the inorganic gas over time was shown.

We found that the O_3 generated in our experiments affect little on the oxidation of α-pinene and the conversion path of the intermediates by comparing the reaction rates of O_3 and OH with α-pinene.

We calculated the rates of reaction of different systems of α-pinene with O_3 and OH, respectively. The corresponding contents are added in the revised supplement (SI Page 11, Lines 236-246; SI Page 18, Lines 276-277). The rate constants of O_3 + α-pinene and OH + α-pinene reactions were determined to be 8.7×10^{-17} and 5.4×10^{-11} cm^3 $molecule^{-1}$ s^{-1}, respectively (Zhang et al., 1992). The reaction rate is calculated as equations (R17) and (R18):

$$v_{O3+\alpha\text{-pinene}} = k_{O3+\alpha\text{-pinene}}[\alpha\text{-pinene}] \quad \text{(R17)}$$

$$v_{OH+\alpha\text{-pinene}} = k_{OH+\alpha\text{-pinene}}[\alpha\text{-pinene}] \quad \text{(R18)}$$

where $v_{O3+\alpha\text{-pinene}}$ and $v_{OH+\alpha\text{-pinene}}$ denote the reaction rate (s^{-1}) of α-pinene with O_3 and OH, respectively. $k_{O3+\alpha\text{-pinene}}$ and $k_{OH+\alpha\text{-pinene}}$ denote the rate constants (cm^3 $molecule^{-1}$ s^{-1}) of the reaction of α-pinene with O_3 and OH, respectively. [α-pinene] and [DMS] denote the measured concentrations of the two VOCs, respectively (cm^3 $molecule^{-1}$).

Figure R5 below demonstrates the trend of the reaction rate with time for different oxidation systems. The rate of reaction between α-pinene and OH has been much greater than that between α-pinene and O_3 during the time period when α-pinene was present. The reaction of O_3 with α-pinene was consistently close to 0. This suggests that O_3 has a negligible effect on the consumption of α-pinene.

Hence, the α-pinene reaction with O_3 would be less important than the reaction with OH in our study.

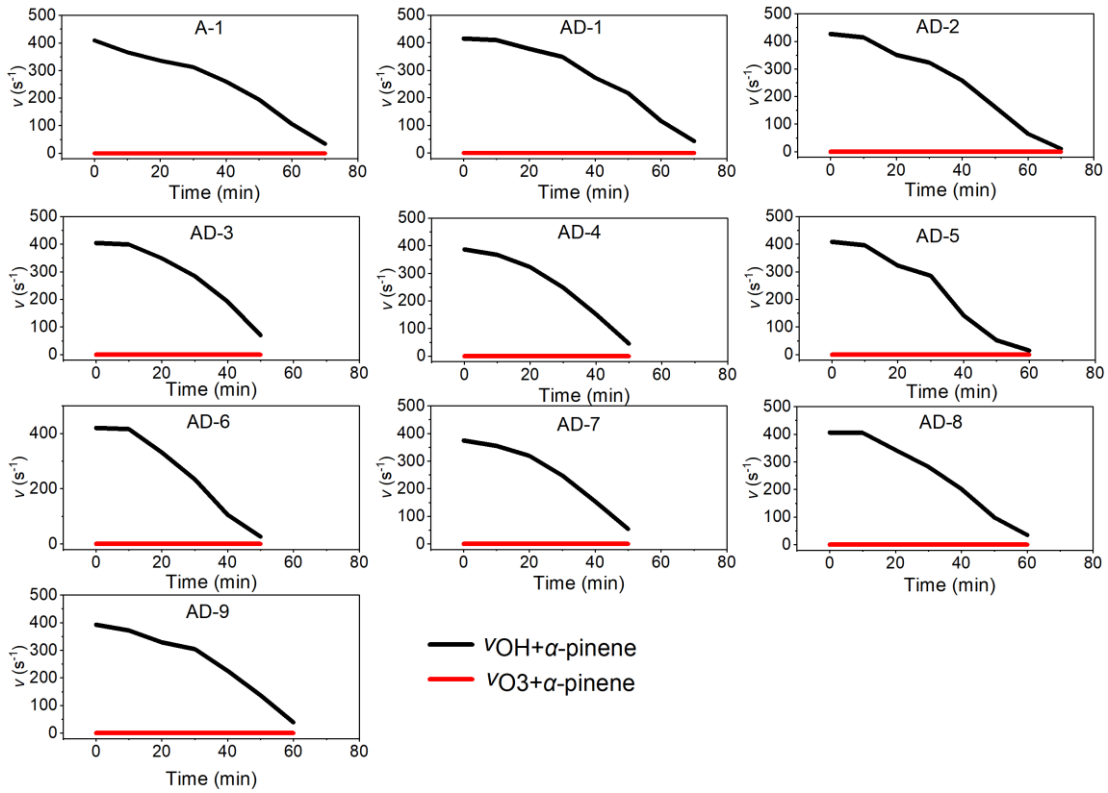

Figure R5. The reaction rate of α-pinene with O_3 or OH in different experiments.

Inorganic gases are described as shown below. The corresponding contents can be found in the revised supplement (SI Pages 5-6, Lines 81-88, 103-106, SI Page 14, Lines 254-255).

Figure S3 shows the reaction profiles of inorganic gases (i.e., NO, NO_x, O_3, and SO_2) over the course of the chamber experiments. NO was consumed more rapidly in the mixed experiments than in Exp. A-1. This is probably due to the higher concentration of RO_2 in the mixed experiments since the oxidation of both DMS and α-pinene produces RO_2 that can react with NO. In addition, it is found that the SO_2 concentration increases with the increasing initial concentration of DMS in the mixed system, which is due to the SO_2 production from DMS photooxidation. However, there is no significant difference in the maximum ozone concentration with increasing DMS, indicating the weak effect of DMS on O_3 production (Chen et al., 2019).

Figure 2 also shows the evolution of the particle mass concentration after the particle wall loss correction. It is demonstrated that the particle mass start to increase before α-pinene has been fully reacted, which is consistent with previous studies (Kari et al., 2017). In addition, the SOA generation occurred after NO is consumed to ~0 ppb due to suppression of hydroperoxide formation by the RO_2 + NO reaction (Liu et al., 2022).

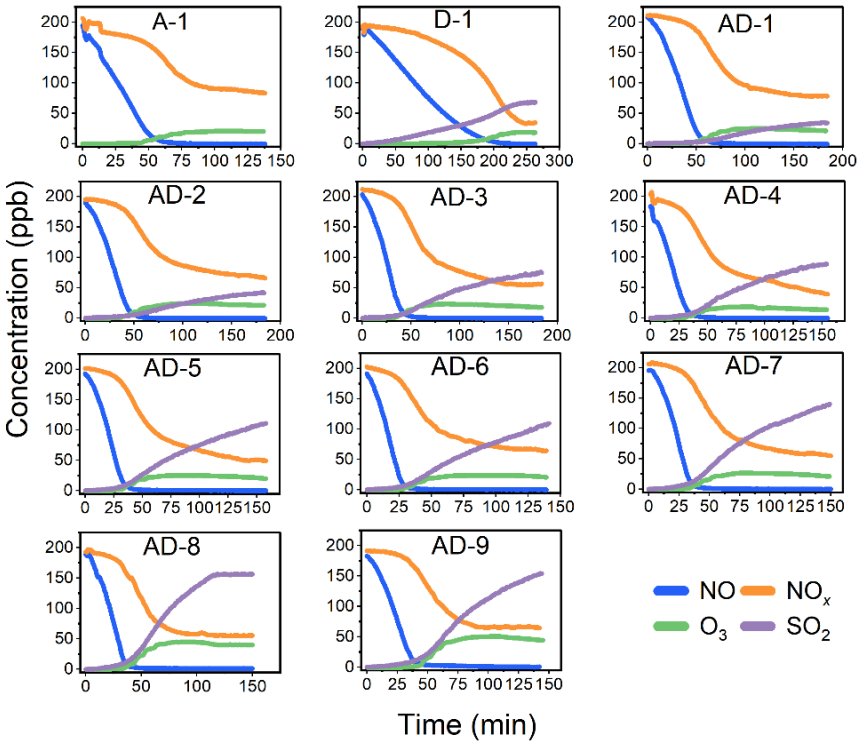

Figure S3. Time profiles of inorganic gases (i.e., NO, NO_x, O_3, and SO_2)

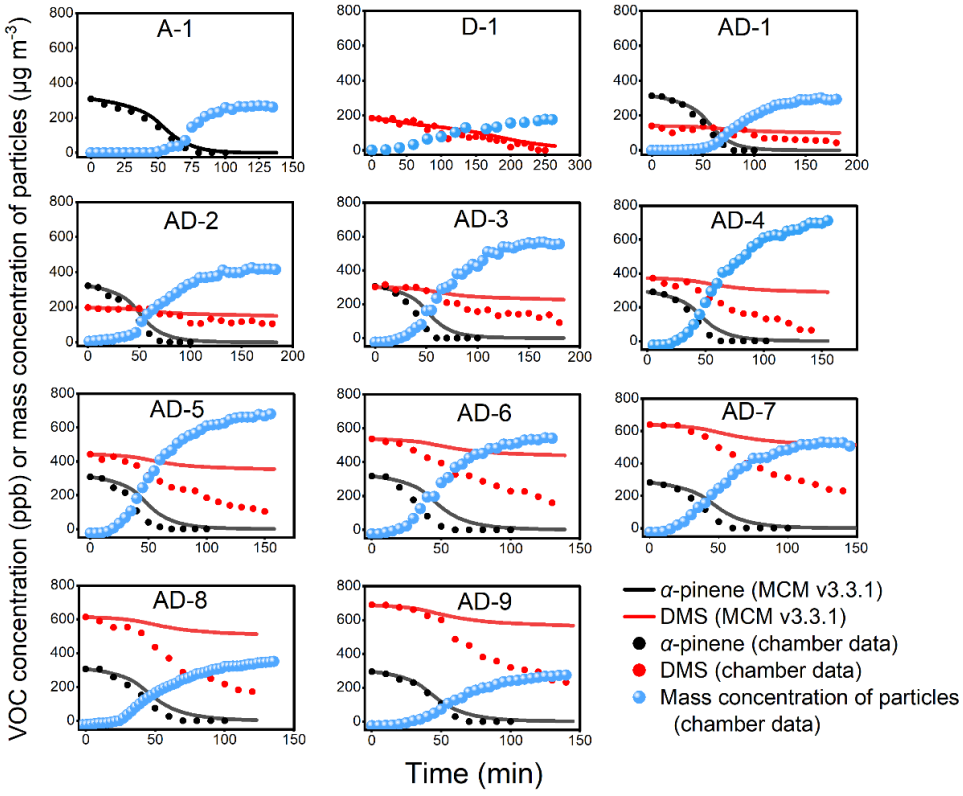

Figure 2. Variation of precursors with reaction time. Red and black dots indicate the results of smog chamber experiments and the curves indicate the results of MCM simulations. Blue dots indicate mass concentration of particles in smog chamber.

We have also added a description of the relevant details in the revised manuscript.

"The time series of inorganic gases and the related presentation of the connection with SOA formation are also presented in Sect. S5 of the supplement." (Page 9, Lines 196-197)

"We calculated the reaction rates of O_3 or OH with α-pinene, respectively. It is shown that the effect of O_3 was very low (Fig. S11). Therefore, the effect of O_3 on the α-pinene SOA is ignored in the discussion. Details can be found in Sect. S10 in the supplement." (Page 11, Lines 235-237)

R2-14:) Table 3: The header of Table 2 is added to the start of Table 3. Please fix this.

A2-14:) We have corrected the header of this table.
Page 9, Line 198 in the revised manuscript.

Table 2. Experimental results of particle-phase components in photooxidation of DMS/α-pinene/NO_x systems.

Exp. No.	[Total particles] [a] μg m^{-3}	[H_2SO_4][b] μg m^{-3}	[MSA][b] μg m^{-3}	[SOA_m][c] μg m^{-3}	Y_m[d]	[SOA_p][e] μg m^{-3}
individual α-pinene						
A-1	269.5	-	-	269.5	0.16±0.02	
individual DMS						
D-1	177.2	50.8	32.83	116.2	0.25±0.03	
mix α-pinene and DMS						
AD-1	296.3	15.0	22.2	270.8	0.14±0.02	216.7
AD-2	422.3	15.7	22.5	400.1	0.20±0.02	270.3
AD-3	572.6	45.4	24.9	507.5	0.24±0.02	425.8
AD-4	714.4	55.4	50.5	607.7	0.25±0.03	648.7
AD-5	683.0	48.8	36.2	613.1	0.24±0.02	708.2
AD-6	551.5	35.3	8.5	504.2	0.19±0.02	680.9
AD-7	539.9	48.4	16.8	476.0	0.19±0.02	677.5
AD-8	364.4	68.7	0.1	237.1	0.08±0.01	537.6
AD-9	289.9	83.2	7.0	154.0	0.06±0.01	436.5

[a] The mass concentration of particles generated by SMPS, corrected for particle wall loss, was calculated as a particle density of 1.2 g cm^{-3}.
[b] IC detection, particle-phase products generated by DMS photooxidation. NH_4^+ was hardly detected. All SO_4^{2-} were detected by IC as H_2SO_4.
[c] The measured SOA mass concentration is expressed as $[\text{Total particles}]_{\text{after-correction}} \times (1 - [H_2SO_4] / [\text{Total particles}]_{\text{before-correction}})$.
[d] $[SOA_m] / (\Delta[\alpha\text{-pinene}] + \Delta[\text{DMS}])$, as mixed yield. Error bars indicate SMPS instrument error of 10%.
[e] The predicted SOA mass concentration by using mass-dependent SOA yields of α-pinene and DMS.

R2-15:) Line 205: Needs citation for the isomerization rate. Additionally, I would recommend reviewing the literature around HPMTF formation as new slower rates exist compared to Wu et al. It is also important to caution the 43% increase in OH with

comments about how much isomerization is occurring in the chamber work presented here. High NO, HO2 and RO2 likely present here could arrest this channel.

A2-15:) Thank you for your valuable suggestion. We reviewed the literature on HPMTF and summarized the isomerization rate of $CH_3SCH_2O_2$ radical in Table R2 below. The temperature range of our experimental setup was 299 ± 1 K, similar to those of (Jacob et al., 2024; Assaf et al., 2023)'s studies. Therefore, we set the isomerization rate of $CH_3SCH_2O_2$ radical to 0.06 s^{-1}. We cite the isomerization rate in the relevant part of the new manuscript.

Table R2. Literature summary of isomerization rates of $CH_3SCH_2O_2$ radicals.

	Rate of isomerization (s^{-1})	**T (K)**	**Ref.**
1	2.1	293	(Wu et al., 2015)
2	0.23 ± 0.12	295 ± 2	(Berndt et al., 2019)
3	0.2	293	(De Jonge et al., 2021)
4	0.041	293	(Veres et al., 2020)
5	0.06 ± 0.02	298	(Jacob et al., 2024; Assaf et al., 2023)

We reviewed the Berndt et al. (2019)' study. Their study showed that a 42% increase in OH occurs when the percentage of isomerization channel exceeds 95%. We revised this in the new manuscript.

We fitted the time series of HO_2, RO_2, NO, and $CH_3SCH_2O_2$ using the modified MCM model. We have added reactions related to the isomerization pathway of the $CH_3SCH_2O_2$ radical to the MCM model. We calculated the rate for each reaction path and evaluated the absolute amount of the isomerization channel of the $CH_3SCH_2O_2$ radical using the MCM model, **see our reply to Comment R2-3 for details.**

Related results are displayed in Fig. R6 and R7 below. As can be seen from Fig. R6, the MCM model results demonstrate the importance of the isomerization channel rate. The rate at which isomerization occurs for the oxidation of DMS alone does not change significantly and rises only slowly after 200 min. However, most of the mixed experiments showed an increase in the slope of the rate of isomerization channel after a reaction time of ~75 min. The isomerization was second important channel that only slower than the NO + $CH_3SCH_2O_2$ reaction. Relative percentage of HO_2, RO_2, NO and isomerization channel of $CH_3SCH_2O_2$ radical further demonstrates this (Fig. R7). Among the four reaction channels, the isomerization pathway of $CH_3SCH_2O_2$ radical accounts for a sufficient percentage to compete with the other bimolecular reaction channels. Therefore, it suggests that isomerization is an important reaction channel of $CH_3SCH_2O_2$ radical, and is not arrested by the high NO, HO_2 and RO_2 concentrations.

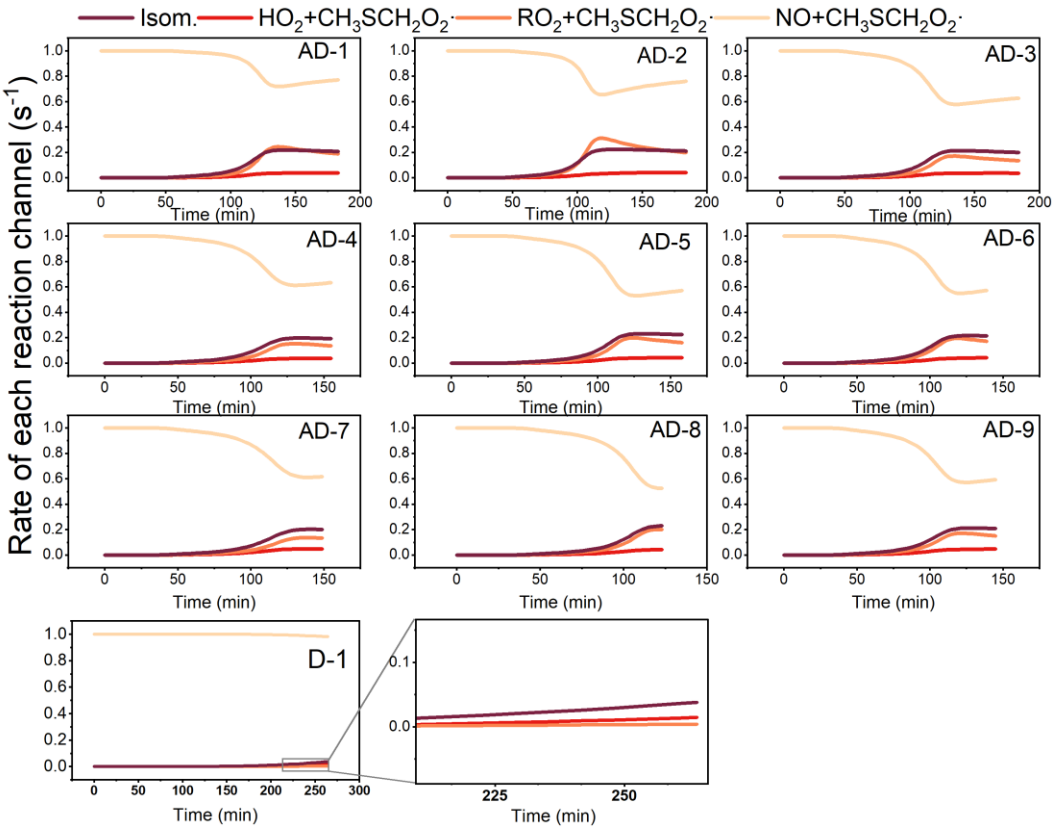

Figure R6. Rates of each reaction channel of the $CH_3SCH_2O_2$ radical calculated by the MCM model in DMS individual and mixed experiments.

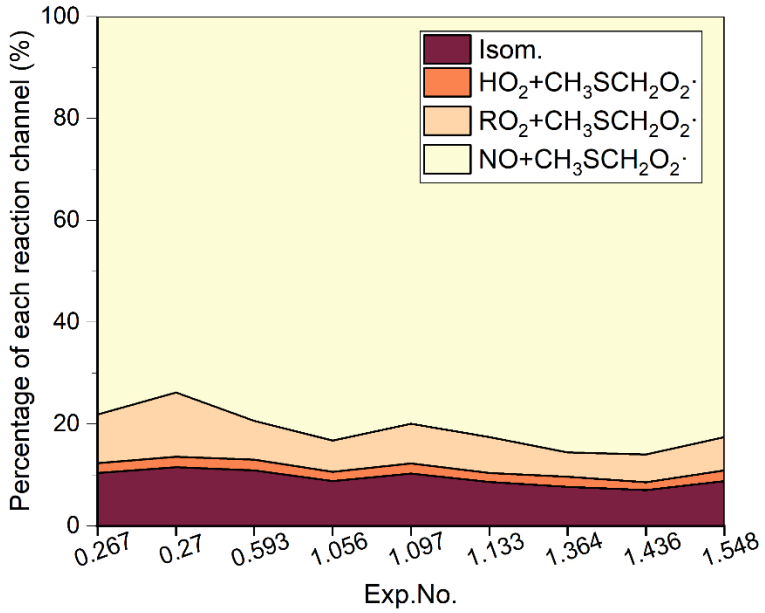

Figure R7. Relative percentage of HO_2, RO_2, NO and isomerization channel of $CH_3SCH_2O_2$ radical obtained from MCM model fitting in different mixing experiments.

The corresponding contents are added in the revised supplement (SI Pages 7-8, Lines 128-141; SI Page 19, Lines 278-280) and manuscript (Page 13, Lines 273-277).

We have also added relevant details about the isomerization channel of DMS in the revised manuscript. As follows:

"As shown in Fig.1, DMS forms $CH_3SCH_2O_2$ radical, which undergoes an isomerization process to form $HOOCH_2SCHO$ product, accompanied by OH regeneration (Berndt et al., 2019; Wu et al., 2015). The isomerization rate of the $CH_3SCH_2O_2$ radical is 0.06 s^{-1} (Assaf et al., 2023; Jacob et al., 2024)." (Page 12, Lines 259-261)

"Their results of atmospheric chemistry simulations demonstrate the predominance ($\geq$ 95%) of $CH_3SCH_2O_2$ isomerization. We fitted the contribution of the different reaction channels of the $CH_3SCH_2O_2$ radical using the MCM model (Fig. 5a). The calculations are detailed in Sec. S7. We find that the isomerization channel is a major reaction channel in our experiments following the NO + $CH_3SCH_2O_2$ channel. (Fig. S12)." (Page 12, Lines 263-267)

R2-16:) Figure 6: "a" and "b" are not labeled on the Figure.

A2-16:) "a" and "b" have been labeled on the Figure in the revised manuscript (Page 16, Lines 341-343).

R2-17:) Figure 7: Please define and describe the meaning of "low, middle, and High" for the mixtures within the description.

A2-17:) "Low, medium and high" represent Δ[DMS]/Δ[α-pinene] in mixed experiments, indicating different mixing ratios. Specifically, "low" represents Exp. AD-10 below the turning point, "medium" represents Exp. AD-11 at the turning point, and "high" represents Exp. AD-12 below the turning point. The corresponding contents are added in the manuscript (Page 17, Lines 363-365).

R2-18:) Figure 8: A hydrogen shift mechanism across 4 carbons is presented and assumed to be a reaction within the chamber. I am not aware of this being a known reaction. Could the authors please provide evidence or citations that would support this mechanism. I understand that the bicyclic nature of the molecule could bring the hydrogen and alkyl radical close, but replacing a secondary radical with a primary seems highly unlikely.

A2-18:) Thank you for your valuable suggestion. We have corrected the mechanisms. We think that the H-shift path shown in Fig. 8 from the original manuscript indeed cannot occur after reviewing the literature. We have removed the second pathway in Fig. 8 from the original manuscript after revision. At the same time, we have modified the first pathway to other pathways, while proposing $C_{10}H_{15}NO_6$ to be the other isomer. The molecular structure of the modified $C_{10}H_{15}NO_6$ is a ring-opening product, which is

oxidized from pinonaldehyde (Eddingsaas et al., 2012a). In addition, we retained the molecular structure of the dimer $C_{20}H_{33}NO_8$, which is derived from Draper et al. (2015). The following texts and figures were added in the revised manuscript.

"Figure 12b shows the possible pathway of ON formation. In the presence of NO_2, the hydrogen atoms on the carbon chain of the typical product pinonaldehyde can be readily oxidized to form nitrogen-containing carboxylate products by the addition of oxygen, i.e., $C_{10}H_{15}NO_6$ (MW 245) (Boyd et al., 2015; Kim et al., 2012; Eddingsaas et al., 2012b)." (Page 20, Lines 417-420)

"In addition, Fig. 12b demonstrates the possible structure of a high molecular weight oligomer generated in the individual α-pinene experiments: $C_{20}H_{33}NO_8$ (MW 415). It is speculated that RO_2 tends more towards isomerization processes such as autoxidation compared to fragmentation reaction (Draper et al., 2015). This pathway increases the possibility of oligomerization of $RO_2 + RO_2$ and $RO_2 + HO_2$ in individual α-pinene oxidation." (Page 20, Lines 423-426)

The mechanisms related to ONs have also been modified, as shown below (Page 21, Lines 427-430).

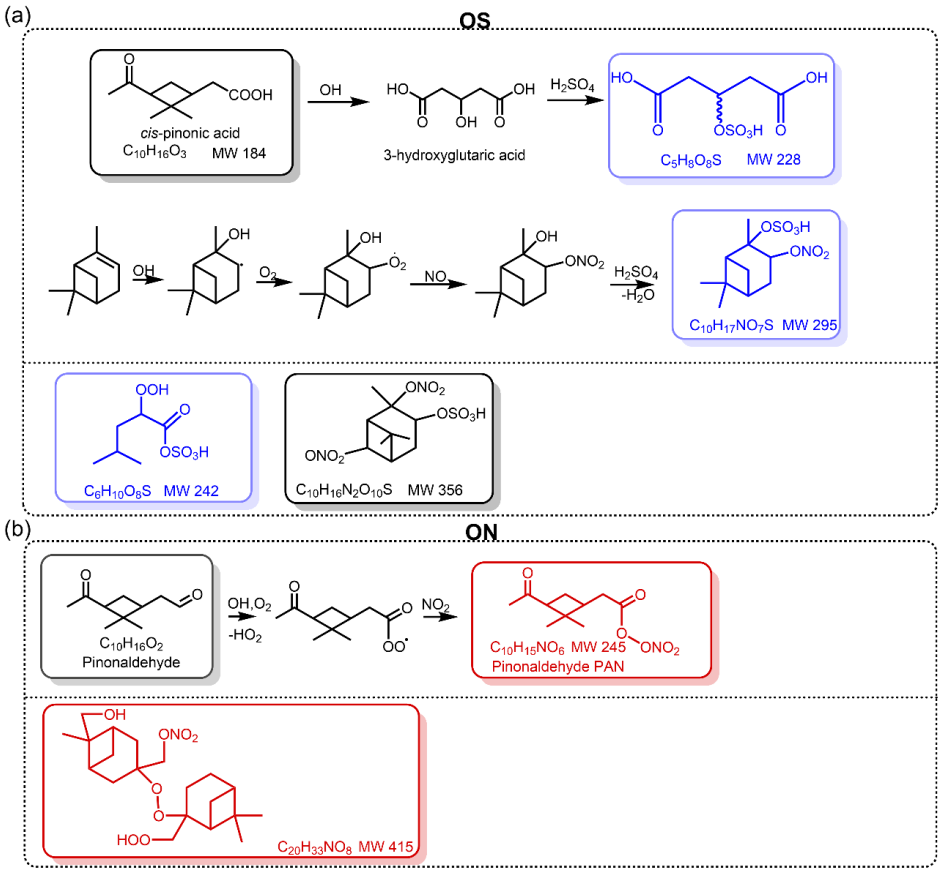

Figure 12. Proposed formation mechanisms and structural for organosulfate (a) and organic nitrates (b) in SOA. Red, blue and black in the boxes refer to the products identified by α-pinene-only SOA products, mixed-only SOA products and α-pinene-mixed-both SOA products, respectively.

References:

Almeida, J., Schobesberger, S., Kürten, A., Ortega, I. K., Kupiainen-Määttä, O., Praplan, A. P., Adamov, A., Amorim, A., Bianchi, F., Breitenlechner, M., David, A., Dommen, J., Donahue, N. M., Downard, A., Dunne, E., Duplissy, J., Ehrhart, S., Flagan, R. C., Franchin, A., Guida, R., Hakala, J., Hansel, A., Heinritzi, M., Henschel, H., Jokinen, T., Junninen, H., Kajos, M., Kangasluoma, J., Keskinen, H., Kupc, A., Kurtén, T., Kvashin, A. N., Laaksonen, A., Lehtipalo, K., Leiminger, M., Leppä, J., Loukonen, V., Makhmutov, V., Mathot, S., McGrath, M. J., Nieminen, T., Olenius, T., Onnela, A., Petäjä, T., Riccobono, F., Riipinen, I., Rissanen, M., Rondo, L., Ruuskanen, T., Santos, F. D., Sarnela, N., Schallhart, S., Schnitzhofer, R., Seinfeld, J. H., Simon, M., Sipilä, M., Stozhkov, Y., Stratmann, F., Tomé, A., Tröstl, J., Tsagkogeorgas, G., Vaattovaara, P., Viisanen, Y., Virtanen, A., Vrtala, A., Wagner, P. E., Weingartner, E., Wex, H., Williamson, C., Wimmer, D., Ye, P., Yli-Juuti, T., Carslaw, K. S., Kulmala, M., Curtius, J., Baltensperger, U., Worsnop, D. R., Vehkamäki, H., and Kirkby, J.: Molecular understanding of sulphuric acid–amine particle nucleation in the atmosphere, Nature, 502, 359-363, 10.1038/nature12663, 2013.

Arquero, K. D., Gerber, R. B., and Finlayson-Pitts, B. J.: The role of oxalic acid in new particle formation from methanesulfonic acid, methylamine, and water, Environ. Sci. Technol., 51, 2124-2130, 10.1021/acs.est.6b05056, 2017.

Assaf, E., Finewax, Z., Marshall, P., Veres, P. R., Neuman, J. A., and Burkholder, J. B.: Measurement of the intramolecular hydrogen-shift rate coefficient for the CH_3SCH_2OO radical between 314 and 433 K, J. Phys. Chem. A, 127, 2336-2350, 10.1021/acs.jpca.2c09095, 2023.

Ayers, G. P., Ivey, J. P., and Gillett, R. W.: Coherence between seasonal cycles of dimethyl sulphide, methanesulphonate and sulphate in marine air, Nature, 349, 404-406, 10.1038/349404a0, 1991.

Ayers, G. P., Cainey, J. M., Granek, H., and Leck, C.: Dimethylsulfide oxidation and the ratio of methanesulfonate to non sea-salt sulfate in the marine aerosol, J. Atmos. Chem., 25, 307-325, 10.1007/BF00053798, 1996.

Barnes, I., Hjorth, J., and Mihalopoulos, N.: Dimethyl sulfide and dimethyl sulfoxide and their oxidation in the atmosphere, Chem. Rev., 37, 10.1002/chin.200624259, 2006.

Bates, T. S., Calhoun, J. A., and Quinn, P. K.: Variations in the methanesulfonate to sulfate molar ratio in submicrometer marine aerosol particles over the south Pacific Ocean, J. Geophys. Res., 97, 9859-9865, 10.1029/92JD00411, 1992.

Berndt, T., Böge, O., Stratmann, F., Heintzenberg, J., and Kulmala, M.: Rapid formation of sulfuric acid particles at near-atmospheric conditions, Science, 307, 698-700, 10.1126/science.1104054, 2005.

Berndt, T., Hoffmann, E. H., Tilgner, A., Stratmann, F., and Herrmann, H.: Direct sulfuric acid formation from the gas-phase oxidation of reduced-sulfur compounds, Nat. Commun., 14, 4849, 10.1038/s41467-023-40586-2, 2023.

Berndt, T., Chen, J., Møller, K. H., Hyttinen, N., Prisle, N. L., Tilgner, A., Hoffmann, E. H., Herrmann, H., and Kjaergaard, H. G.: SO_2 formation and peroxy radical isomerization in the atmospheric reaction of OH radicals with dimethyl disulfide, Chem. Comm., 56, 13634-13637, 10.1039/D0CC05783E, 2020.

Berndt, T., Scholz, W., Mentler, B., Fischer, L., Hoffmann, E. H., Tilgner, A., Hyttinen, N., Prisle, N. L., Hansel, A., and Herrmann, H.: Fast peroxy radical isomerization and OH recycling in the reaction of OH radicals with dimethyl sulfide, J. Phys. Chem. Lett., 10, 6478-6483, 10.1021/acs.jpclett.9b02567, 2019.

Bloss, C., Wagner, V., Jenkin, M. E., Volkamer, R., Bloss, W. J., Lee, J. D., Heard, D. E., Wirtz, K., Martin-Reviejo, M., Rea, G., Wenger, J. C., and Pilling, M. J.: Development of a detailed chemical mechanism (MCMv3.1) for the atmospheric oxidation of aromatic hydrocarbons, Atmos. Chem. Phys., 5, 641-664, 10.5194/acp-5-641-2005, 2005.

Boyd, C. M., Sanchez, J., Xu, L., Eugene, A. J., Nah, T., Tuet, W. Y., Guzman, M. I., and Ng, N. L.: Secondary organic aerosol formation from the β-pinene + NO_3 system: Effect of humidity and peroxy radical fate, Atmos. Chem. Phys., 15, 7497-7522, 10.5194/acp-15-7497-2015, 2015.

Cala, B. A., Archer-Nicholls, S., Weber, J., Abraham, N. L., Griffiths, P. T., Jacob, L., Shin, Y. M., Revell, L. E., Woodhouse, M., and Archibald, A. T.: Development, intercomparison, and evaluation of an improved mechanism for the oxidation of dimethyl sulfide in the UKCA model, Atmos. Chem. Phys., 23, 14735-14760, 10.5194/acp-23-14735-2023, 2023.

Chen, J., Berndt, T., Møller, K. H., Lane, J. R., and Kjaergaard, H. G.: Atmospheric fate of the CH_3SOO radical from the $CH_3S + O_2$ equilibrium, J. Phys. Chem. A, 125, 8933-8941, 10.1021/acs.jpca.1c06900, 2021.

Chen, L., Wang, J., Gao, Y., Xu, G., Yang, X., Lin, Q., and Zhang, Y.: Latitudinal distributions of atmospheric MSA and MSA/nss-SO_4^{2-} ratios in summer over the high latitude regions of the Southern and Northern Hemispheres, J. Atmos. Chem., 117, 10.1029/2011JD016559, 2012.

Chen, T. and Jang, M.: Secondary organic aerosol formation from photooxidation of a mixture of dimethyl sulfide and isoprene, Atmos. Environ., 46, 271-278, 10.1016/j.atmosenv.2011.09.082, 2012.

Chen, T., Liu, Y., Ma, Q., Chu, B., Zhang, P., Liu, C., Liu, J., and He, H.: Significant source of secondary aerosol: Formation from gasoline evaporative emissions in the presence of SO_2 and NH_3, Atmos. Chem. Phys., 19, 8063-8081, 10.5194/acp-19-8063-2019, 2019.

Coates, J. and Butler, T. M.: A comparison of chemical mechanisms using tagged ozone production potential (TOPP) analysis, Atmos. Chem. Phys., 15, 8795-8808, 10.5194/acp-15-8795-2015, 2015.

Crounse, J. D., Nielsen, L. B., Jørgensen, S., Kjaergaard, H. G., and Wennberg, P. O.: Autoxidation of organic compounds in the atmosphere, J. Phys. Chem. Lett., 4, 3513-3520, 10.1021/jz4019207, 2013.

D'Ambro, E. L., Møller, K. H., Lopez-Hilfiker, F. D., Schobesberger, S., Liu, J., Shilling, J. E., Lee, B. H., Kjaergaard, H. G., and Thornton, J. A.: Isomerization of second-generation isoprene peroxy radicals: Epoxide formation and implications for secondary organic aerosol yields, Environ. Sci. Technol., 51, 4978-4987, 10.1021/acs.est.7b00460, 2017.

De Jonge, W. R., Elm, J., Rosati, B., Christiansen, S., Hyttinen, N., Lüdemann, D., Bilde, M., and Roldin, P.: Secondary aerosol formation from dimethyl sulfide – improved mechanistic understanding based on smog chamber experiments and modelling, Atmos. Chem. Phys., 21, 9955-9976, 10.5194/acp-21-9955-2021, 2021.

Draper, D. C., Farmer, D. K., Desyaterik, Y., and Fry, J. L.: A qualitative comparison of secondary organic aerosol yields and composition from ozonolysis of monoterpenes at varying concentrations of NO_2, Atmos. Chem. Phys., 15, 12267-12281, 10.5194/acp-15-12267-2015, 2015.

Eddingsaas, N. C., Loza, C. L., Yee, L. D., Seinfeld, J. H., and Wennberg, P. O.: α-Pinene photooxidation under controlled chemical conditions – Part 1: Gas-phase composition in low- and high-NO_x environments, Atmos. Chem. Phys., 12, 6489-6504, 10.5194/acp-12-6489-2012, 2012a.

Eddingsaas, N. C., Loza, C. L., Yee, L. D., Chan, M., Schilling, K. A., Chhabra, P. S., Seinfeld, J. H., and Wennberg, P. O.: α-Pinene photooxidation under controlled chemical conditions – Part 2: SOA yield and composition in low- and high-NO_x environments, Atmos. Chem. Phys., 12, 7413-7427, 10.5194/acp-12-7413-2012, 2012b.

Ehn, M., Thornton, J. A., Kleist, E., Sipilä, M., Junninen, H., Pullinen, I., Springer, M., Rubach, F., Tillmann, R., Lee, B., Lopez-Hilfiker, F., Andres, S., Acir, I.-H., Rissanen, M., Jokinen, T., Schobesberger, S., Kangasluoma, J., Kontkanen, J., Nieminen, T., Kurtén, T., Nielsen, L. B., Jørgensen, S., Kjaergaard, H. G., Canagaratna, M., Maso, M. D., Berndt, T., Petäjä, T., Wahner, A., Kerminen, V.-M., Kulmala, M., Worsnop, D. R., Wildt, J., and Mentel, T. F.: A large source of low-volatility secondary organic aerosol, Nature, 506, 476-479, 10.1038/nature13032, 2014.

Fry, J. L., Draper, D. C., Zarzana, K. J., Campuzano-Jost, P., Day, D. A., Jimenez, J. L., Brown, S. S., Cohen, R. C., Kaser, L., Hansel, A., Cappellin, L., Karl, T., Hodzic Roux, A., Turnipseed, A., Cantrell, C., Lefer, B. L., and Grossberg, N.: Observations of gas- and aerosol-phase organic nitrates at BEACHON-RoMBAS 2011, Atmos. Chem. Phys., 13, 8585-8605, 10.5194/acp-13-8585-2013, 2013.

Fung, K. M., Heald, C. L., Kroll, J. H., Wang, S., Jo, D. S., Gettelman, A., Lu, Z., Liu, X., Zaveri, R. A., Apel, E. C., Blake, D. R., Jimenez, J. L., Campuzano-Jost, P., Veres, P. R., Bates, T. S., Shilling, J. E., and Zawadowicz, M.: Exploring dimethyl sulfide (DMS) oxidation and implications for global aerosol radiative forcing, Atmos. Chem. Phys., 22, 1549-1573, 10.5194/acp-22-1549-2022, 2022.

Gaston, C. J., Pratt, K. A., Qin, X., and Prather, K. A.: Real-time detection and mixing state of methanesulfonate in single particles at an inland urban location during a phytoplankton bloom, Environ. Sci. Technol., 44, 1566-1572, 10.1021/es902069d, 2010.

Jacob, L. S. D., Giorio, C., and Archibald, A. T.: Extension, development, and evaluation of the representation of the OH-initiated dimethyl sulfide (DMS) oxidation mechanism in the Master Chemical Mechanism (MCM) v3.3.1 framework, Atmos. Chem. Phys., 24, 3329-3347, 10.5194/acp-24-3329-2024, 2024.

Jernigan, C. M., Fite, C. H., Vereecken, L., Berkelhammer, M. B., Rollins, A. W., Rickly, P. S., Novelli, A., Taraborrelli, D., Holmes, C. D., and Bertram, T. H.: Efficient production of carbonyl sulfide in the low-NO_x oxidation of dimethyl sulfide, Geophys. Res. Lett., 49, e2021GL096838, 10.1029/2021GL096838, 2022.

Kari, E., Hao, L., Yli-Pirilä, P., Leskinen, A., Kortelainen, M., Grigonyte, J., Worsnop, D. R., Jokiniemi, J., Sippula, O., Faiola, C. L., and Virtanen, A.: Effect of pellet boiler exhaust on secondary organic aerosol formation from α-pinene, Environ. Sci. Technol., 51, 1423-1432, 10.1021/acs.est.6b04919, 2017.

Kim, H., Barkey, B., and Paulson, S. E.: Real refractive indices and formation yields of secondary organic aerosol generated from photooxidation of limonene and α-pinene: The effect of the HC/NO_x ratio, J. Phys. Chem. A, 116, 6059–6067, 10.1021/jp301302z.s001, 2012.

Kirkby, J., Curtius, J., Almeida, J., Dunne, E., Duplissy, J., Ehrhart, S., Franchin, A., Gagné, S., Ickes, L., Kürten, A., Kupc, A., Metzger, A., Riccobono, F., Rondo, L., Schobesberger, S., Tsagkogeorgas, G., Wimmer, D., Amorim, A., Bianchi, F., Breitenlechner, M., David, A., Dommen, J., Downard, A., Ehn, M., Flagan, R. C., Haider, S., Hansel, A., Hauser, D., Jud, W., Junninen, H., Kreissl, F., Kvashin, A., Laaksonen, A., Lehtipalo, K., Lima, J., Lovejoy, E. R., Makhmutov, V., Mathot, S., Mikkilä, J., Minginette, P., Mogo, S., Nieminen, T., Onnela, A., Pereira, P., Petäjä, T., Schnitzhofer, R., Seinfeld, J. H., Sipilä, M., Stozhkov, Y., Stratmann, F., Tomé, A., Vanhanen, J., Viisanen, Y., Vrtala, A., Wagner, P. E., Walther, H., Weingartner, E., Wex, H., Winkler, P. M., Carslaw, K. S., Worsnop, D. R., Baltensperger, U., and Kulmala, M.: Role of sulphuric acid, ammonia and galactic cosmic rays in atmospheric aerosol nucleation, Nature, 476, 429-433, 10.1038/nature10343, 2011.

Kirkby, J., Duplissy, J., Sengupta, K., Frege, C., Gordon, H., Williamson, C., Heinritzi, M., Simon, M., Yan, C., Almeida, J., Tröstl, J., Nieminen, T., Ortega, I. K., Wagner, R., Adamov, A., Amorim, A., Bernhammer, A.-K., Bianchi, F., Breitenlechner, M., Brilke, S., Chen, X., Craven, J., Dias, A., Ehrhart, S., Flagan, R. C., Franchin, A., Fuchs, C., Guida, R., Hakala, J., Hoyle, C. R., Jokinen, T., Junninen, H., Kangasluoma, J., Kim, J., Krapf, M., Kürten, A., Laaksonen, A., Lehtipalo, K., Makhmutov, V., Mathot, S., Molteni, U., Onnela, A., Peräkylä, O., Piel, F., Petäjä, T., Praplan, A. P., Pringle, K., Rap, A., Richards, N. A. D., Riipinen, I., Rissanen, M. P., Rondo, L., Sarnela, N., Schobesberger, S., Scott, C. E., Seinfeld, J. H., Sipilä, M., Steiner, G., Stozhkov, Y., Stratmann, F., Tomé, A., Virtanen, A., Vogel, A. L., Wagner, A. C., Wagner, P. E.,

Weingartner, E., Wimmer, D., Winkler, P. M., Ye, P., Zhang, X., Hansel, A., Dommen, J., Donahue, N. M., Worsnop, D. R., Baltensperger, U., Kulmala, M., Carslaw, K. S., and Curtius, J.: Ion-induced nucleation of pure biogenic particles, Nature, 533, 521-526, 10.1038/nature17953, 2016.

Knote, C., Tuccella, P., Curci, G., Emmons, L., Orlando, J. J., Madronich, S., Baró, R., Jiménez-Guerrero, P., Luecken, D., Hogrefe, C., Forkel, R., Werhahn, J., Hirtl, M., Pérez, J. L., San José, R., Giordano, L., Brunner, D., Yahya, K., and Zhang, Y.: Influence of the choice of gas-phase mechanism on predictions of key gaseous pollutants during the AQMEII phase-2 intercomparison, Atmos. Environ., 115, 553-568, 10.1016/j.atmosenv.2014.11.066, 2015.

Lewandowski, M., Jaoui, M., Offenberg, J. H., Krug, J. D., and Kleindienst, T. E.: Atmospheric oxidation of isoprene and 1,3-butadiene: Influence of aerosol acidity and relative humidity on secondary organic aerosol, Atmos. Chem. Phys., 15, 3773-3783, 10.5194/acp-15-3773-2015, 2015.

Liu, C., Liu, J., Liu, Y., Chen, T., and He, H.: Secondary organic aerosol formation from the OH-initiated oxidation of guaiacol under different experimental conditions, Atmos. Environ., 207, 30-37, 10.1016/j.atmosenv.2019.03.021, 2019.

Liu, J., D'Ambro, E. L., Lee, B. H., Schobesberger, S., Bell, D. M., Zaveri, R. A., Zelenyuk, A., Thornton, J. A., and Shilling, J. E.: Monoterpene photooxidation in a continuous-flow chamber: SOA yields and impacts of oxidants, NO_x, and VOC precursors, Environ. Sci. Technol., 56, 12066-12076, 10.1021/acs.est.2c02630, 2022.

Liu, S., Jia, L., Xu, Y., Tsona, N. T., Ge, S., and Du, L.: Photooxidation of cyclohexene in the presence of SO_2: SOA yield and chemical composition, Atmos. Chem. Phys., 17, 13329-13343, 10.5194/acp-17-13329-2017, 2017.

Liu, T., Wang, X., Hu, Q., Deng, W., Zhang, Y., Ding, X., Fu, X., Bernard, F., Zhang, Z., Lü, S., He, Q., Bi, X., Chen, J., Sun, Y., Yu, J., Peng, P., Sheng, G., and Fu, J.: Formation of secondary aerosols from gasoline vehicle exhaust when mixing with SO_2, Atmos. Chem. Phys., 16, 675-689, 10.5194/acp-16-675-2016, 2016.

Lv, G., Zhang, C., and Sun, X.: Understanding the oxidation mechanism of methanesulfinic acid by ozone in the atmosphere, Sci. Rep., 9, 322, 10.1038/s41598-018-36405-0, 2019.

Mao, J., Ren, X., Brune, W. H., Olson, J. R., Crawford, J. H., Fried, A., Huey, L. G., Cohen, R. C., Heikes, B., Singh, H. B., Blake, D. R., Sachse, G. W., Diskin, G. S., Hall, S. R., and Shetter, R. E.: Airborne measurement of OH reactivity during INTEX-B, Atmos. Chem. Phys., 9, 163-173, 10.5194/acp-9-163-2009, 2009.

Martin, S. T., Artaxo, P., Machado, L. A. T., Manzi, A. O., Souza, R. A. F., Schumacher, C., Wang, J., Andreae, M. O., Barbosa, H. M. J., Fan, J., Fisch, G., Goldstein, A. H., Guenther, A., Jimenez, J. L., Pöschl, U., Silva Dias, M. A., Smith, J. N., and Wendisch, M.: Introduction: Observations and modeling of the Green Ocean Amazon (GoAmazon2014/5), Atmos. Chem. Phys., 16, 4785-4797, 10.5194/acp-16-4785-2016, 2016.

Martin, S. T., Artaxo, P., Machado, L., Manzi, A. O., Souza, R. A. F., Schumacher, C., Wang, J., Biscaro, T., Brito, J., Calheiros, A., Jardine, K., Medeiros, A., Portela, B., de Sá, S. S., Adachi, K., Aiken, A. C., Albrecht, R., Alexander, L., Andreae, M. O., Barbosa, H. M. J., Buseck, P., Chand, D., Comstock, J. M., Day, D. A., Dubey, M., Fan, J., Fast, J., Fisch, G., Fortner, E., Giangrande, S., Gilles, M., Goldstein, A. H., Guenther, A., Hubbe, J., Jensen, M., Jimenez, J. L., Keutsch, F. N., Kim, S., Kuang, C., Laskin, A., McKinney, K., Mei, F., Miller, M., Nascimento, R., Pauliquevis, T., Pekour, M., Peres, J., Petäjä, T., Pöhlker, C., Pöschl, U., Rizzo, L., Schmid, B., Shilling, J. E., Dias, M. A. S., Smith, J. N., Tomlinson, J. M., Tóta, J., and Wendisch, M.: The Green Ocean Amazon experiment (GoAmazon2014/5) observes pollution affecting gases, aerosols, clouds, and rainfall over the rain forest, Bull. Amer. Meteor. Soc., 98, 981-997, 10.1175/BAMS-D-15-00221.1, 2017.

Mauldin III, R. L., Tanner, D. J., Heath, J. A., Huebert, B. J., and Eisele, F. L.: Observations of H_2SO_4 and MSA during PEM-Tropics-A, J. Geophys. Res., 104, 5801-5816, 10.1029/98JD02612, 1999.

Metzger, A., Dommen, J., Gaeggeler, K., Duplissy, J., Prevot, A. S. H., Kleffmann, J., Elshorbany, Y., Wisthaler, A., and Baltensperger, U.: Evaluation of 1,3,5 trimethylbenzene degradation in the detailed tropospheric chemistry mechanism, MCMv3.1, using environmental chamber data, Atmos. Chem. Phys., 8, 6453-6468, 10.5194/acp-8-6453-2008, 2008.

Ng, N. L., Kroll, J. H., Chan, A. W. H., Chhabra, P. S., Flagan, R. C., and Seinfeld, J. H.: Secondary organic aerosol formation from m-xylene, toluene, and benzene, Atmos. Chem. Phys., 7, 3909-3922, 10.5194/acp-7-3909-2007, 2007.

Nguyen, T. B., Crounse, J. D., Schwantes, R. H., Teng, A. P., Bates, K. H., Zhang, X., St. Clair, J. M., Brune, W. H., Tyndall, G. S., Keutsch, F. N., Seinfeld, J. H., and Wennberg, P. O.: Overview of the focused isoprene eXperiment at the California Institute of technology (FIXCIT): Mechanistic chamber studies on the oxidation of biogenic compounds, Atmos. Chem. Phys., 14, 13531-13549, 10.5194/acp-14-13531-2014, 2014.

Ortega, A. M., Hayes, P. L., Peng, Z., Palm, B. B., Hu, W., Day, D. A., Li, R., Cubison, M. J., Brune, W. H., Graus, M., Warneke, C., Gilman, J. B., Kuster, W. C., de Gouw, J., Gutiérrez-Montes, C., and Jimenez, J. L.: Real-time measurements of secondary organic aerosol formation and aging from ambient air in an oxidation flow reactor in the Los Angeles area, Atmos. Chem. Phys., 16, 7411-7433, 10.5194/acp-16-7411-2016, 2016.

Peng, Z., Lee-Taylor, J., Orlando, J. J., Tyndall, G. S., and Jimenez, J. L.: Organic peroxy radical chemistry in oxidation flow reactors and environmental chambers and their atmospheric relevance, Atmos. Chem. Phys., 19, 813-834, 10.5194/acp-19-813-2019, 2019.

Peng, Z., Day, D. A., Ortega, A. M., Palm, B. B., Hu, W., Stark, H., Li, R., Tsigaridis, K., Brune, W. H., and Jimenez, J. L.: Non-OH chemistry in oxidation flow reactors for

the study of atmospheric chemistry systematically examined by modeling, Atmos. Chem. Phys., 16, 4283-4305, 10.5194/acp-16-4283-2016, 2016.

Praske, E., Otkjær, R. V., Crounse, J. D., Hethcox, J. C., Stoltz, B. M., Kjaergaard, H. G., and Wennberg, P. O.: Atmospheric autoxidation is increasingly important in urban and suburban North America, Proc. Natl. Acad. Sci., 115, 64-69, 10.1073/pnas.1715540115, 2018.

Robinson, A. L., Donahue, N. M., Shrivastava, M. K., Weitkamp, E. A., Sage, A. M., Grieshop, A. P., Lane, T. E., Pierce, J. R., and Pandis, S. N.: Rethinking organic aerosols: Semivolatile emissions and photochemical aging, Science, 315, 1259-1262, 10.1126/science.1133061, 2007.

Ryerson, T. B., Andrews, A. E., Angevine, W. M., Bates, T. S., Brock, C. A., Cairns, B., Cohen, R. C., Cooper, O. R., de Gouw, J. A., Fehsenfeld, F. C., Ferrare, R. A., Fischer, M. L., Flagan, R. C., Goldstein, A. H., Hair, J. W., Hardesty, R. M., Hostetler, C. A., Jimenez, J. L., Langford, A. O., McCauley, E., McKeen, S. A., Molina, L. T., Nenes, A., Oltmans, S. J., Parrish, D. D., Pederson, J. R., Pierce, R. B., Prather, K., Quinn, P. K., Seinfeld, J. H., Senff, C. J., Sorooshian, A., Stutz, J., Surratt, J. D., Trainer, M., Volkamer, R., Williams, E. J., and Wofsy, S. C.: The 2010 California research at the nexus of air quality and climate change (CalNex) field study, J. Geophys. Res. Atmos., 118, 5830-5866, 10.1002/jgrd.50331, 2013.

Sarrafzadeh, M., Wildt, J., Pullinen, I., Springer, M., Kleist, E., Tillmann, R., Schmitt, S. H., Wu, C., Mentel, T. F., Zhao, D., Hastie, D. R., and Kiendler-Scharr, A.: Impact of NO_x and OH on secondary organic aerosol formation from β-pinene photooxidation, Atmos. Chem. Phys., 16, 11237-11248, 10.5194/acp-16-11237-2016, 2016.

Shen, J., Scholz, W., He, X.-C., Zhou, P., Marie, G., Wang, M., Marten, R., Surdu, M., Rörup, B., Baalbaki, R., Amorim, A., Ataei, F., Bell, D. M., Bertozzi, B., Brasseur, Z., Caudillo, L., Chen, D., Chu, B., Dada, L., Duplissy, J., Finkenzeller, H., Granzin, M., Guida, R., Heinritzi, M., Hofbauer, V., Iyer, S., Kemppainen, D., Kong, W., Krechmer, J. E., Kürten, A., Lamkaddam, H., Lee, C. P., Lopez, B., Mahfouz, N. G. A., Manninen, H. E., Massabò, D., Mauldin, R. L., Mentler, B., Müller, T., Pfeifer, J., Philippov, M., Piedehierro, A. A., Roldin, P., Schobesberger, S., Simon, M., Stolzenburg, D., Tham, Y. J., Tomé, A., Umo, N. S., Wang, D., Wang, Y., Weber, S. K., Welti, A., Wollesen de Jonge, R., Wu, Y., Zauner-Wieczorek, M., Zust, F., Baltensperger, U., Curtius, J., Flagan, R. C., Hansel, A., Möhler, O., Petäjä, T., Volkamer, R., Kulmala, M., Lehtipalo, K., Rissanen, M., Kirkby, J., El-Haddad, I., Bianchi, F., Sipilä, M., Donahue, N. M., and Worsnop, D. R.: High gas-phase methanesulfonic acid production in the OH-initiated oxidation of dimethyl sulfide at low temperatures, Environ. Sci. Technol., 56, 13931-13944, 10.1021/acs.est.2c05154, 2022.

Sipilä, M., Berndt, T., Petäjä, T., Brus, D., Vanhanen, J., Stratmann, F., Patokoski, J., Mauldin, R. L., Hyvärinen, A.-P., Lihavainen, H., and Kulmala, M.: The role of sulfuric acid in atmospheric nucleation, Science, 327, 1243-1246, 10.1126/science.1180315, 2010.

Stone, D., Whalley, L. K., and Heard, D. E.: Tropospheric OH and HO_2 radicals: Field measurements and model comparisons, Chem. Soc. Rev., 41, 6348-6404, 10.1039/C2CS35140D, 2012.

Veres, P. R., Neuman, J. A., Bertram, T. H., Assaf, E., Wolfe, G. M., Williamson, C. J., Weinzierl, B., Tilmes, S., Thompson, C. R., Thames, A. B., Schroder, J. C., Saiz-Lopez, A., Rollins, A. W., Roberts, J. M., Price, D., Peischl, J., Nault, B. A., Møller, K. H., Miller, D. O., Meinardi, S., Li, Q., Lamarque, J.-F., Kupc, A., Kjaergaard, H. G., Kinnison, D., Jimenez, J. L., Jernigan, C. M., Hornbrook, R. S., Hills, A., Dollner, M., Day, D. A., Cuevas, C. A., Campuzano-Jost, P., Burkholder, J., Bui, T. P., Brune, W. H., Brown, S. S., Brock, C. A., Bourgeois, I., Blake, D. R., Apel, E. C., and Ryerson, T. B.: Global airborne sampling reveals a previously unobserved dimethyl sulfide oxidation mechanism in the marine atmosphere, Proc. Natl. Acad. Sci., 117, 4505-4510, 10.1073/pnas.1919344117, 2020.

Vivanco, M. G., Santiago, M., Sánchez, M., Clavero, M. A., Borrás, E., Ródenas, M., Alacreu, F., Vázquez, M., Clemente, E., Porras, R., Muñoz, A., and Stein, A.: Experimental data on SOA formation from mixtures of anthropogenic and biogenic organic compounds, Atmosfera, 26, 59-73, 10.1016/S0187-6236(13)71062-2, 2013.

Wang, N., Jorga, S. D., Pierce, J. R., Donahue, N. M., and Pandis, S. N.: Particle wall-loss correction methods in smog chamber experiments, Atmos. Meas. Tech., 11, 6577-6588, 10.5194/amt-11-6577-2018, 2018.

Wildt, J., Mentel, T. F., Kiendler-Scharr, A., Hoffmann, T., Andres, S., Ehn, M., Kleist, E., Müsgen, P., Rohrer, F., Rudich, Y., Springer, M., Tillmann, R., and Wahner, A.: Suppression of new particle formation from monoterpene oxidation by NO_x, Atmos. Chem. Phys., 14, 2789-2804, 10.5194/acp-14-2789-2014, 2014.

Wu, R., Wang, S., and Wang, L.: New mechanism for the atmospheric oxidation of dimethyl sulfide. The importance of intramolecular hydrogen shift in a CH_3SCH_2OO radical, J. Phys. Chem. A, 119, 112-117, 10.1021/jp511616j, 2015.

Wu, S., Lü, Z., Hao, J., Zhao, Z., Li, J., Takekawa, H., Minoura, H., and Yasuda, A.: Construction and characterization of an atmospheric simulation smog chamber, Adv. Atmos. Sci., 24, 250-258, 10.1007/s00376-007-0250-3, 2007.

Xu, L., Du, L., Tsona, N. T., and Ge, M.: Anthropogenic effects on biogenic secondary organic aerosol formation, Adv. Atmos. Sci., 38, 1053-1084, 10.1007/s00376-020-0284-3, 2021.

Xu, L., Møller, K. H., Crounse, J. D., Otkjær, R. V., Kjaergaard, H. G., and Wennberg, P. O.: Unimolecular reactions of peroxy radicals formed in the oxidation of α-pinene and β-pinene by hydroxyl radicals, J. Phys. Chem. A, 123, 1661-1674, 10.1021/acs.jpca.8b11726, 2019.

Yang, X., Yuan, B., Peng, Z., Peng, Y., Wu, C., Yang, S., Li, J., and Shao, M.: Inter-comparisons of VOC oxidation mechanisms based on box model: A focus on OH reactivity, J. Environ. Sci., 114, 286-296, 10.1016/j.jes.2021.09.002, 2022.

Ye, J., Abbatt, J. P. D., and Chan, A. W. H.: Novel pathway of SO_2 oxidation in the atmosphere: Reactions with monoterpene ozonolysis intermediates and secondary organic aerosol, Atmos. Chem. Phys., 18, 5549-5565, 10.5194/acp-18-5549-2018, 2018.

Ye, Q., Goss, M. B., Krechmer, J. E., Majluf, F., Zaytsev, A., Li, Y., Roscioli, J. R., Canagaratna, M., Keutsch, F. N., Heald, C. L., and Kroll, J. H.: Product distribution, kinetics, and aerosol formation from the OH oxidation of dimethyl sulfide under different RO_2 regimes, Atmos. Chem. Phys., 22, 16003-16015, 10.5194/acp-22-16003-2022, 2022.

Ye, Q., Goss, M. B., Isaacman-VanWertz, G., Zaytsev, A., Massoli, P., Lim, C., Croteau, P., Canagaratna, M., Knopf, D. A., Keutsch, F. N., Heald, C. L., and Kroll, J. H.: Organic sulfur products and peroxy radical isomerization in the OH oxidation of dimethyl sulfide, ACS Earth Space Chem., 5, 2013-2020, 10.1021/acsearthspacechem.1c00108, 2021.

Zhang, R., Khalizov, A., Wang, L., Hu, M., and Xu, W.: Nucleation and growth of nanoparticles in the atmosphere, Chem. Rev., 112, 1957-2011, 10.1021/cr2001756, 2012.

Zhang, S.-H., Shaw, M., Seinfeld, J. H., and Flagan, R. C.: Photochemical aerosol formation from α-pinene and β-pinene, J. Geophys. Res. , 97, 20717-20729, doi.org/10.1029/92JD02156, 1992.

Zhang, Y., Cheng, M., Gao, J., and Li, J.: Review of the influencing factors of secondary organic aerosol formation and aging mechanism based on photochemical smog chamber simulation methods, J. Environ. Sci., 123, 545-559, doi.org/10.1016/j.jes.2022.10.033, 2023.

Ziemann, P. J. and Atkinson, R.: Kinetics, products, and mechanisms of secondary organic aerosol formation, Chem. Soc. Rev., 41, 6582-6605, 10.1039/C2CS35122F, 2012.

Zong, R., Xue, L., Wang, T., and Wang, W.: Inter-comparison of the regional atmospheric chemistry mechanism (RACM2) and master chemical mechanism (MCM) on the simulation of acetaldehyde, Atmos. Environ., 186, 144-149, 10.1016/j.atmosenv.2018.05.013, 2018.